*Citation:* Padel, M., Clausen, S., Poujol, M., Álvaro, J.J., 2022. Shifts in the Ediacaran to Lower Ordovician sedimentary zircon provenances of Northwest Gondwana: the Pyrenean files. Geologica Acta, 20.14, 1-18, I-VIII.
DOI: 10.1344/GeologicaActa2022.20.14

geologica acta

# Shifts in the Ediacaran to Lower Ordovician sedimentary zircon provenances of Northwest Gondwana: the Pyrenean files

**Maxime Padel[1] Sébastien Clausen[2] Marc Poujol[3] J. Javier Álvaro[4]**

[1]**Bureau de Rercherche Géologique et Minière (BRGM), Direction des Géoressources (DGR), BP36009**
45060 Orléans E-mail: m.padel @brgm.fr

[2]**University of Lille, Centre National de la Recherche Scientifique (CNRS), Unité Mixte de Recherche (UMR) 8198 - Evo-Eco-Paleo**
F-59000 Lille, France. E-mail: sebastien.clausen@univ-lille1.fr

[3]**University of Rennes, CNRS, Géosciences Rennes**
UMR 6118, 35000 Rennes, France. E-mail: marc.poujol@univ-rennes1.fr

[4]**Instituto de Geociencias (CSIC-UCM)**
Dr. Severo Ochoa 7, 28040 Madrid, Spain. E-mail: jj.alvaro@csic.es

## ABSTRACT

Detrital zircon grains from Cambrian–Lower Ordovician sandstones and quartzites sampled in the Pyrenees were dated by LA-ICPMS in order to assess their provenance sources. Resulting age distributions are compared to other available datasets from neighbouring margins, such as Morocco, the Iberian Peninsula, southern France and Sardinia. Kolmogorov-Smirnov (K-S) test and Crystallization Age-Depositional Age (CA-DA) diagrams were used to compare zircon populations estimating their possible correlation with the arc/rift/drift geodynamic evolution of the northwestern Gondwana margin. During Terreneuvian times, zircon populations allowed the distinction of i) a southwesternmost edge (Atlas-Ossa-Morena Rift) mostly influenced by Panafrican and Anti-Atlasian sources (ca. 0.63–0.54), ii) a northeasternmost edge (Sardinia) recording the influence of the Saharan Metacraton and the Arabian Nubian Shield, with an distinct Stenian–Tonian shift (ca. 1.25–0.85Ga) and iii) an intermediate palaeogeographic transect, where lies the Central Iberian, West Asturian-Leonese and Cantabrian Zones, the Montagne Noire and the Pyrenees sharing similar populations and a chronologically progressive influence from Anti-Atlasian/Panafrican to Saharan Metacraton/Arabian Nubian Shield sources. This gradual modification in zircon percentage populations supports similar trends based on climatically sensitive indicators, biogeographic patterns of Cambrian Epoch 2 archaeocyathan and microfossil assemblages, and laterally correlatable episodes of carbonate production, all of them pointing to a Cambrian setting for the Pyrenean Basin between the Montagne Noire (Occitan Domain) and the Sardinian margins of NW Gondwana. The Terreneuvian zircon patterns recorded in the Pyrenees gradually evolved from Cambrian Epoch 2 to Early Ordovician times, reflecting the geodynamic evolution from Panafrican and Cadomian arc-related to rift-dominant conditions. During Furongian and Ordovician times, the relative percentage of zircon populations led to a more spread age curve, characteristic of extensional settings and pointing to rift (passive margin) conditions.

***KEYWORDS*** **Orogeny. Rift. Palaeogeography. Pyrenees. Detrital zircon. Gondwana.**

## INTRODUCTION

Detrital zircon U-Pb geochronology is a powerful tool to characterize crustal growth episodes, deciphering detrital sources, estimating the maximum depositional age of strata, and constraining the geodynamic evolution of continental margins (*e.g.* Gehrels, 2014). During the two last decades, the analysis of zircon provenances has been regularly applied to identify the different sources of the Neoproterozoic–early Palaeozoic basins fringing Northwest Gondwana in order to determine their relative proximity to different orogens (*e.g.* Altumi *et al.*, 2013; Avigad *et al.*, 2012, 2018; Ballouard *et al.*, 2018; Couzinié *et al.*, 2019; Drost *et al.*, 2011; Fernández-Suárez *et al.*, 2014; Gutiérrez-Alonso *et al.*, 2003; Kydonakis *et al.*, 2014; Linnemann *et al.*, 2008; Margalef *et al.*, 2016; Meinhold *et al.*, 2011, 2013; Padel *et al.*, 2017a,b, 2018; Pastor-Galán *et al.*, 2013; Shaw *et al.*, 2014). Among these orogenic events, the Neoproterozoic Panafrican (Anti-Atlas, 790–560Ma), Cadomian (*e.g.* Armorican Massif, Iberia and Bohemian Massif, 850–550Ma) and Avalonian (*e.g.* Newfoundland, New England, Nova Scotia and Cape Breton, 730–570Ma) events have received particular attention as they share a broad shift from convergent to extensional conditions, with a turnover close to the Ediacaran–Cambrian boundary interval (590–540Ma; Ballèvre *et al.*, 2001; Blein *et al.*, 2014a, b; Linnemann *et al.*, 2007; Murphy *et al.*, 1999; Nance *et al.*, 2002; Stampfi and von Raumer, 2008; Stampfi *et al.*, 2013 ).

In NW Gondwana (including the Moroccan Anti-Atlas, the Iberian Peninsula, southern France and Sardinia), evidences for this arc/rift geodynamic change are preserved in disconnected basement exposures of the European Variscan Belt (Fig. 1A). In southwestern Europe, the Variscan Ibero-Armorican Arc contains two branches (Ballèvre *et al.*, 2009; Martínez Catalán *et al.*, 2007; Pouclet *et al.*, 2017): i) a southwestern branch represented by the Iberian Massif and ii) a northeastern branch that includes the Armorican Massif, the South Armorican Domain (southwestern Britany and Vendée), the northern Massif Central, the Occitan Domain (Albigeois, Montagne Noire, Mouthoumet, and Cévennes massifs of the southern Massif Central) and its lateral prolongation into the Pyrenean Domain, Corsica and Sardinia. Although the Pyrenees share strong Ediacaran–Cambrian stratigraphic similarities with the Cantabrian Zone, the Montagne Noire and SW Sardinia, its Cambrian palaeogeographic position has been an everlasting matter of discussion (Álvaro *et al.*, 2014a; Ballèvre *et al.*, 2009; Laumonier *et al.*, 1996, 2004; Pouclet *et al.*, 2017). As a result, the palaeogeographic position of the Pyrenees is often questioned or even omitted in many Ediacaran–early Palaeozoic palaeogeographic reconstructions of Gondwana (*e.g.* Murphy *et al.*, 2004; Nance *et al.*, 2008).

This study aims to assess the evolution, across space and time, of the influence of sedimentary zircon populations during Cambrian–Early Ordovician times throughout a palaeogeographic SW-NE transect of NW Gondwana. It focuses on successions from the Anti-Atlas (Morocco), the Ossa-Morena, Central Iberian, West Asturian-Leonese and Cantabrian Zones of the Iberian Massif, the central and eastern Pyrenees (France/Spain border), the Montagne Noire (France) and southern Sardinia (Italy). We present here a comprehensive study of detrital zircon grains from Cambrian sandstones and quartzites in the Pyrenees, completed with other Ediacaran and Ordovician samples from the Pyrenees analysed by Casas *et al.* (2015), Margalef *et al.* (2016) and Padel *et al.* (2018). Our study is based on a multi-tool analysis of Kernel density plots (KDE), statistical Kolmogorov-Smirnov (K-S) tests and Crystallization Age-Depositional Age (CA-DA) diagrams, which leads to the proposal of new palaeogeographic constrains for the geodynamic evolution of NW Gondwana during Ediacaran to Ordovician times.

## GEOLOGICAL SETTING AND STRATIGRAPHY OF THE PYRENEES

The basement of south-western Europe includes, among others, the core of the Iberian and Armorican massifs, the French Massif Central and the Pyrenees. Recent palaeogeographic re-appraisals based on litho- (Padel *et al.*, 2018) and biostratigraphic revisions (Wallet *et al.*, 2022), completed with correlations of the mid–Ordovician Sardic Phase (Álvaro *et al.*, 2020 and references within) have placed the Ediacaran–Ordovician Pyrenean margin of Gondwana as a lateral continuity of neighbouring domains, such as the Occitan Domain (including Montagne Noire and the Mouthoumet massifs) and SW Sardinia. As a result, the Cambrian Pyrenean Basin has been recently integrated in the reconstruction of pre–Variscan palaeogeographic puzzles along NW Gondwana, after combining structural, magmatic and stratigraphic comparisons (*e.g.* Álvaro *et al.*, 2021; Casas and Murphy, 2018).

The present-day Pyrenean Belt formed as an intracontinental fold and thrust belt related to a Late Cretaceous to Early Neogene collision between the Iberian microplate and the southern European plate. The belt is subdivided into three E–W morphostructural units, the Northern, Axial and Southern zones (Barnolas and Chiron, 1996). The Axial Zone consists of a complete Ediacaran to Carboniferous succession intruded by Ordovician granites, which include distinct migmatized orthogneiss aureoles, and Variscan anatectic granites (Casas *et al.*, 2010; Castiñeiras *et al.*, 2008; Cocherie *et al.*, 2005; Deloule *et al.*, 2002; Denèle *et al.*, 2009; Lemirre *et al.*, 2019; Liesa *et al.*, 2011; Martínez *et al.*, 2011; Mezger and Gerdes, 2016).

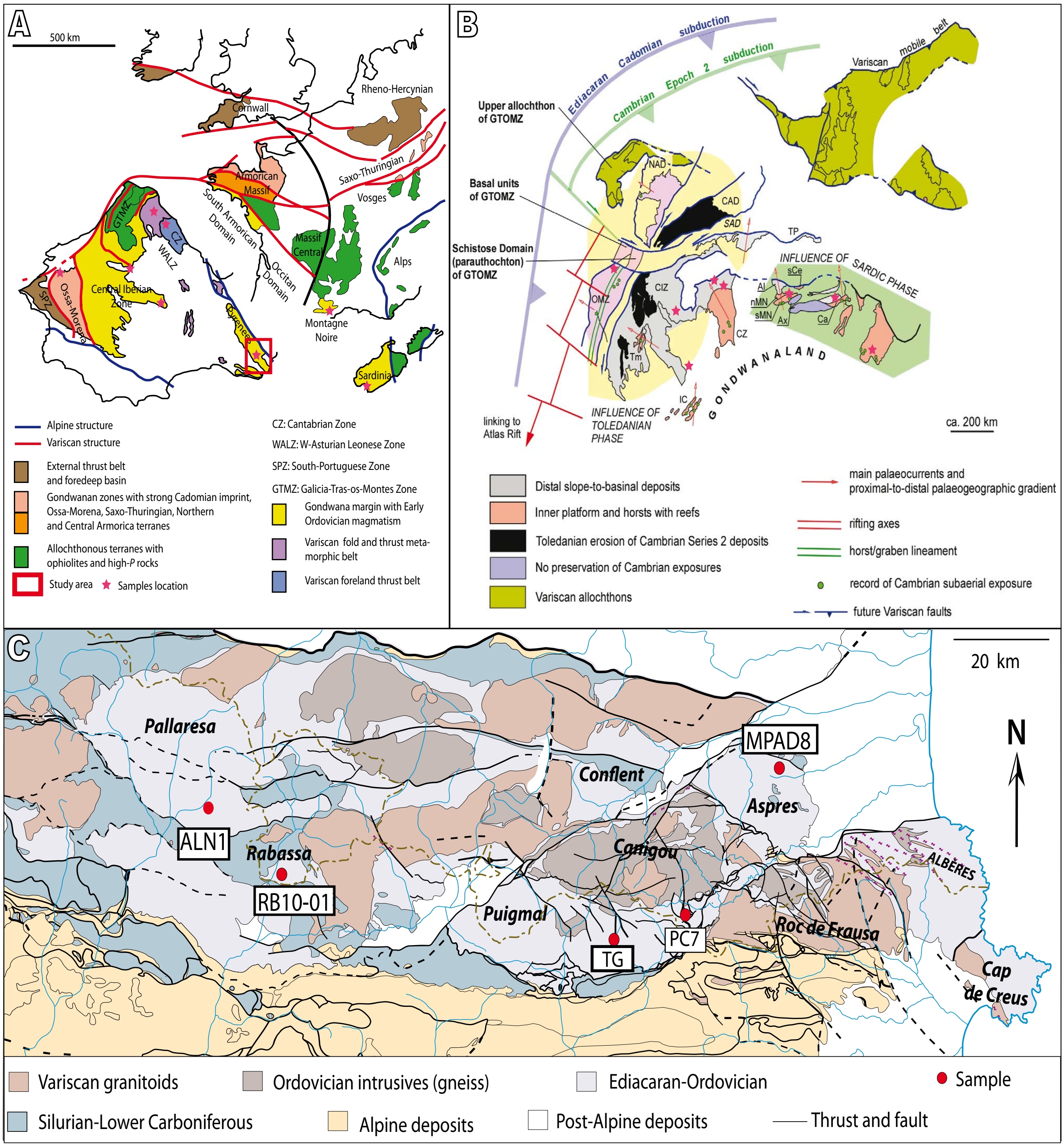


**FIGURE 1.** A) Geological sketch of the Variscan Belt in southwestern Europe with tectonostratigraphic domains including Cambrian–Ordovician exposures from peri-Gondwana; modified after Ballèvre *et al.* (2009), Martinez-Catalán (2007) and Pouclet *et al.* (2017). B) Early Palaeozoic palaeogeographic reconstruction of different basement domains in SW Europe, based on Álvaro *et al.* (2021). Al= Albigeois Mountains; Ax= Montagne Noire Axial Zone; Ca= Canigó Massif; CAD= Central Armorican Domain; CIZ= Central Iberian Zone; CZ= Cantabrian Zone; GTOMZ= Galicia-Trás-os-Montes Zone; IC= Iberian Chains; NAD= North Armorican Domain; nMN= northern Montagne Noire; OMZ= Ossa-Morena Zone; sCE= southern Cévennes; sMN= southern Montagne Noire; Tm= Toledo Mountains. C) Geological map of the eastern Pyrenees (Red squared in A) with setting of studied samples; modified after Padel *et al.* (2018).

The metamorphic domes resulting from the Variscan orogeny are surrounded by various metamorphic grades affecting the entire pre–Variscan strata (*e.g.* Cochelin *et al.*, 2018; Fig. 1C). The Axial Zone is bounded by the North- and South-Pyrenean Thrusts (Laumonier *et al.*, 2015), subsequently flanked by post–Variscan-dominant series.

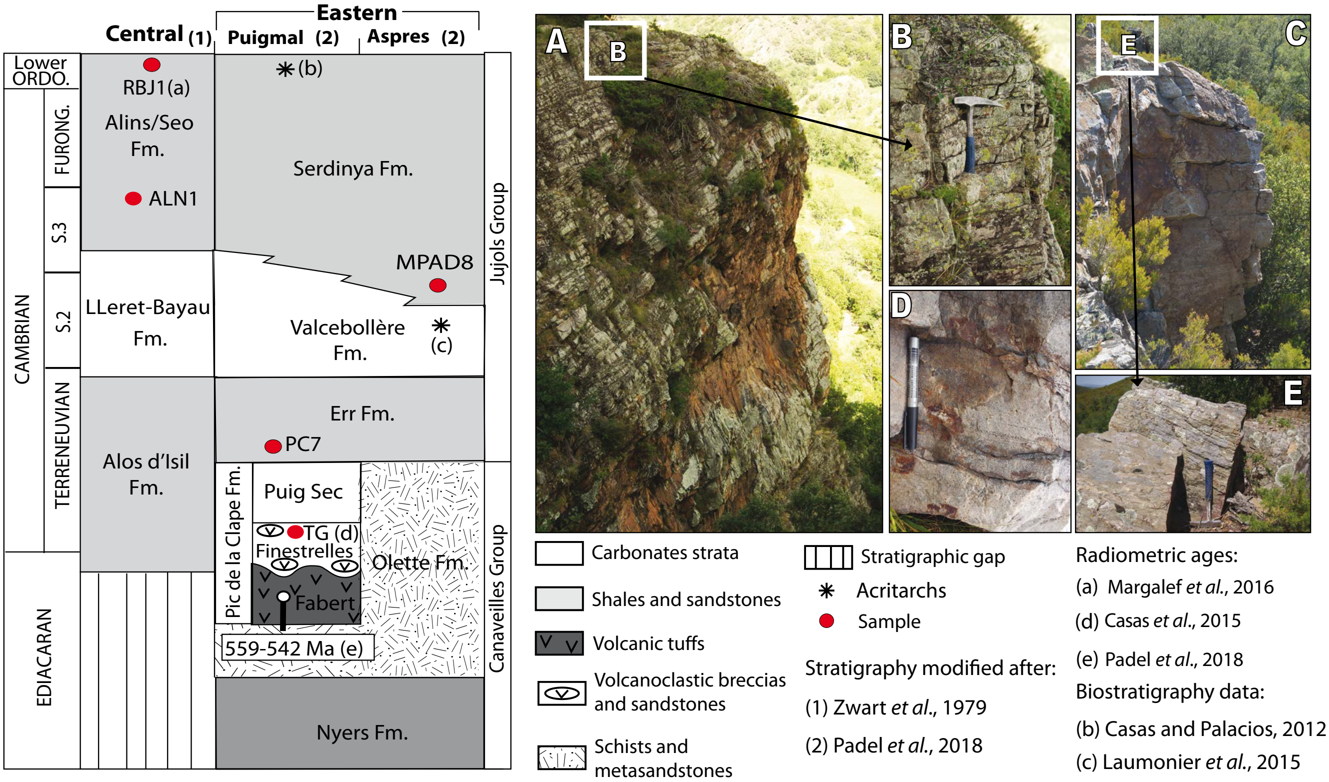


**FIGURE 2.** Ediacaran–Lower Ordovician stratigraphic chart of the central and eastern Pyrenees with locations of studied samples (red circles). A) Picture with location of the meta-sandstone where sample ALN1 where extracted. B) Zoom on the location of sample ALN1. C) Picture with location of the meta-sandstone where sample MPAD8 was extracted. D) Picture of the meta-sandstone where sample PC7 was selected. E) Detail of the location of sample MPAD8.

Pre–Variscan rocks mostly crop out in the central and eastern Axial Zone, from the Pallaresa Dome to the Mediterranean Sea (Fig. 1C). In the eastern Pyrenees, several tectonostratigraphic units are recognized, such as the Puigmal, Conflent, Aspres, Roc de Frausa, Albera and Cap de Creus units (Fig. 1C). Their Ediacaran–Lower Ordovician succession is subdivided into the Canaveilles and Jujols groups (Laumonier *et al.*, 1996, 2004; Padel *et al.*, 2018; Fig. 2). The Ediacaran Canaveilles Group, 2–3km thick, is a monotonous micaschist-dominant succession locally punctuated by rhyolites, volcanosedimentary breccias, marbles and quartzites. The presence/absence of carbonate interbeds allows deciphering between the (lower) Nyers and the (upper) Olette formations. The latter is capped, in the Puigmal tectonostratigraphic unit (Padel *et al.*, 2018) (Fig 2), by a volcanosedimentary complex, up to 500m in thickness, named Pic de la Clape Formation, where three members have been distinguished: i) the Fabert Member, a succession of bedded metarhyolites, up to 50m thick, interbedded with intraformational breccias, arkoses, shales and basic lava flow interbeds; ii) the Finestrelles Member, a package of massive felsic-dominant ignimbrites and volcanosedimentary breccias, up to 500m thick, interbedded with tuffaceous sandstones and siltstones, and locally punctuated by pristine-to-volcaniclastic limestone interbeds and iii) the Pic de la Clape Formation, up to 180m thick, composed of massive to bedded limestones and marbles (Padel *et al.*, 2018). The overlying Miaolingian–Lower Ordovician Jujols Group has an estimated thickness of 3–4km and comprises, from bottom to top, the Err, Valcebollère and Serdinya formations. The Err Formation, ~1500m thick, consists of shale/metasandstone alternations, conformably overlain by the massive to bedded limestones and marbles of the Valcebollère Formation, 200-300m thick. Finally, the Serdinya Formation, ~2000m thick, consists of homogeneous micaschists and shales, irregularly punctuated by centimetre to decimetre-thick sandstone interbeds (Casas and Palacios, 2012).

In the Pallaresa dome of the central Pyrenees, a thick (>4000m) siliciclastic-dominant succession can be subdivided into three units, named the Alos d'Isil, Lleret-Bayau and Alins formations (Laumonier *et al.*, 1996), which represent the three-fold subdivision of the Jujols Group reported above. In the Rabassa Unit, the same succession is represented by the Seo Formation, a lithostratigraphic equivalent to both the Serdinya and Alins Formations (Figs. 1; 2).

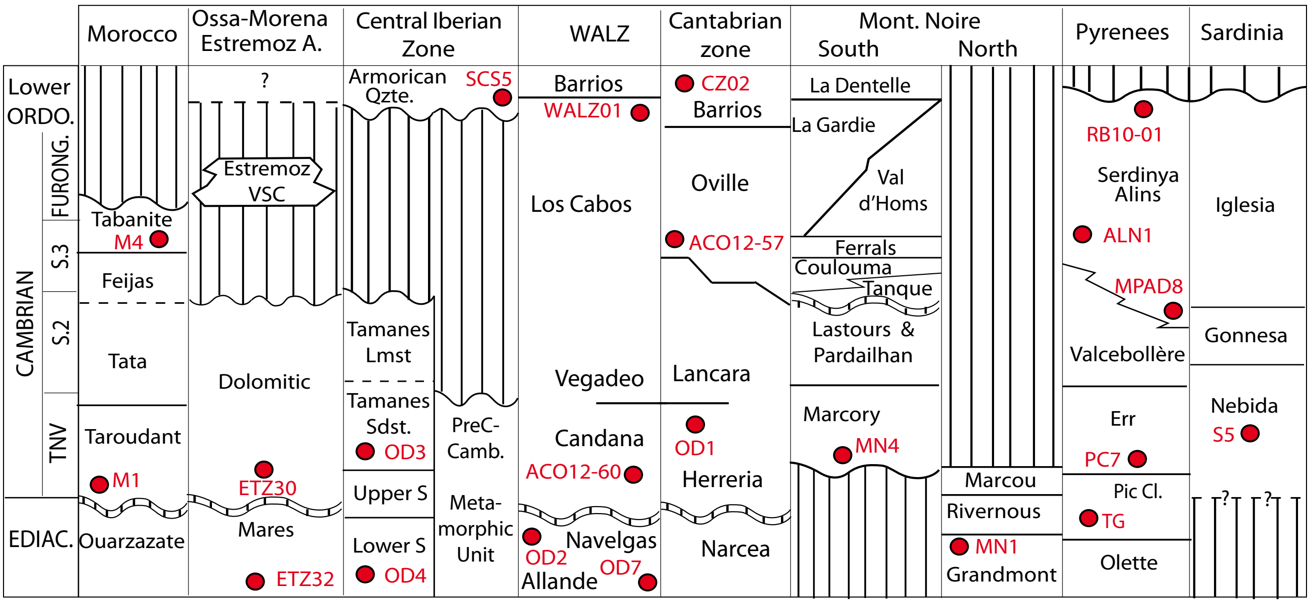


**FIGURE 3.** Schematic Ediacaran–Lower Ordovician stratigraphic chart showing setting of samples reported in this study: Avigad *et al.* (2012: samples M1 and M4, Anti-Atlas, Morocco and sample S5, SW Sardinia, Italy), Pereira *et al.* (2012: ETZ30 and ETZ32, Ossa-Morena Zone, Spain); Fernández-Suárez *et al.* (2014: OD3 and OD4, Central-Iberian Zone; OD2 and OD7, West Asturian-Leonese Zone; OD1, Cantabrian Zone, Spain); Shaw et al. (2014: SCS5, Central Iberian Zone; WALZ01, West Asturian-Leonese Zone; CZ02, Cantabrian Zone, Spain); Henderson *et al.* (2016: ACO12-57 and ACO12-60, Cantabrian Zone, Spain); Casas *et al.* (2015: TG0701, TG0702, TG0703 summarized under sample TG because of their sampling from a single lithostratigraphic unit, Spain); Padel *et al.* (2017: MN4, Montagne Noire, France (Figs. 6; 7). S= Series; Qtze.= Quartzite; VSC= volcanosedimentary complex; Estremoz A= Estremoz Anticline; Sdst.= Sandstone and Lmst.= limestone

## MATERIAL AND METHODS

Three fine- to medium-grained sandstones were sampled in the Pyrenean Axial Zone for U-Pb detrital zircon geochronology: i) sample PC7 from a Terreneuvian Err metasandstone in the Puigmal Unit; ii) MPAD8 from a lowermost Serdinya metasandstone (encompassing the Cambrian Series 2–3 transition) in the Aspres Unit and iii) ALN1 from a Miaolingian Alins metasandstone in the central Pyrenees (Figs. 1; 2). Former U-Pb detrital zircon analyses were performed by Margalef *et al.* (2016) in sample RB-10-01, from a Lower Ordovician sandstone of the Seo Formation in the Rabassa Unit, central Pyrenees.

These four datasets are compared with previous analyses from Ediacaran to Ordovician detrital zircon grains following a SW-NE transect along the northwestern Gondwana margin (Fig. 3). The sample selection was based on i) distinct chronostratigraphic controls, ii) representative amounts of zircon grains to be statically acceptable for comparison and iii) precise sample location within the regional tectonostratigraphic units. The compilation includes over 50 samples but, based on the three discerning criteria stated above, only 19 samples were selected. These include case studies from the Moroccan Anti-Atlas (Avigad *et al.*, 2012: samples M1 and M4), the Ossa-Morena Zone (Pereira *et al.*, 2012: ETZ30 and ETZ32), the Central Iberian Zone (Fernández-Suárez *et al.*, 2014: OD3 and OD4; Shaw *et al.*, 2014: SCS5), the West Asturian-Leonese Zone (Fernández-Suárez *et al.*, 2014: OD2 and OD7; Shaw *et al.*, 2014: WALZ01), the Cantabrian Zone (Fernández-Suárez *et al.*, 2014: OD1; Shaw *et al.*, 2014: CZ02; Henderson *et al.*, 2016: ACO12-57 and ACO12-60), the Montagne Noire (Padel *et al.*, 2017a: MN4, MN1), the eastern Pyrenees (Casas *et al.*, 2015: TG0701, TG0702 and TG0703, named below sample TG because the three sandstones were sampled in the same structural and lithostratigraphic unit), and southern Sardinia (Avigad *et al.*, 2012: S5) (Fig. 3). Assignation of these samples to potential sedimentary sources follow the nomenclature reported by Avigad *et al.* (2003, 2012), Linnemann *et al.* (2011), Drost *et al.* (2011) and Pereira *et al.* (2012).

### U-Pb analytical method

The zircon grains yielded by the new Pyrenean samples (PC7, MPAD8 and ALN1) were randomly hand-picked under a binocular microscope after grinding of fresh rocks followed by heavy liquid and magnetic separation. They were included in epoxy resin and then polished in order to expose their inner parts. Internal growth textures and morphologies of zircon grains were revealed using cathodoluminescence and back-scattered electron imaging under Scanning Electron Microscope (SEM) at the Laboratoire Océanologie et Géoscience of the University of Lille 1.

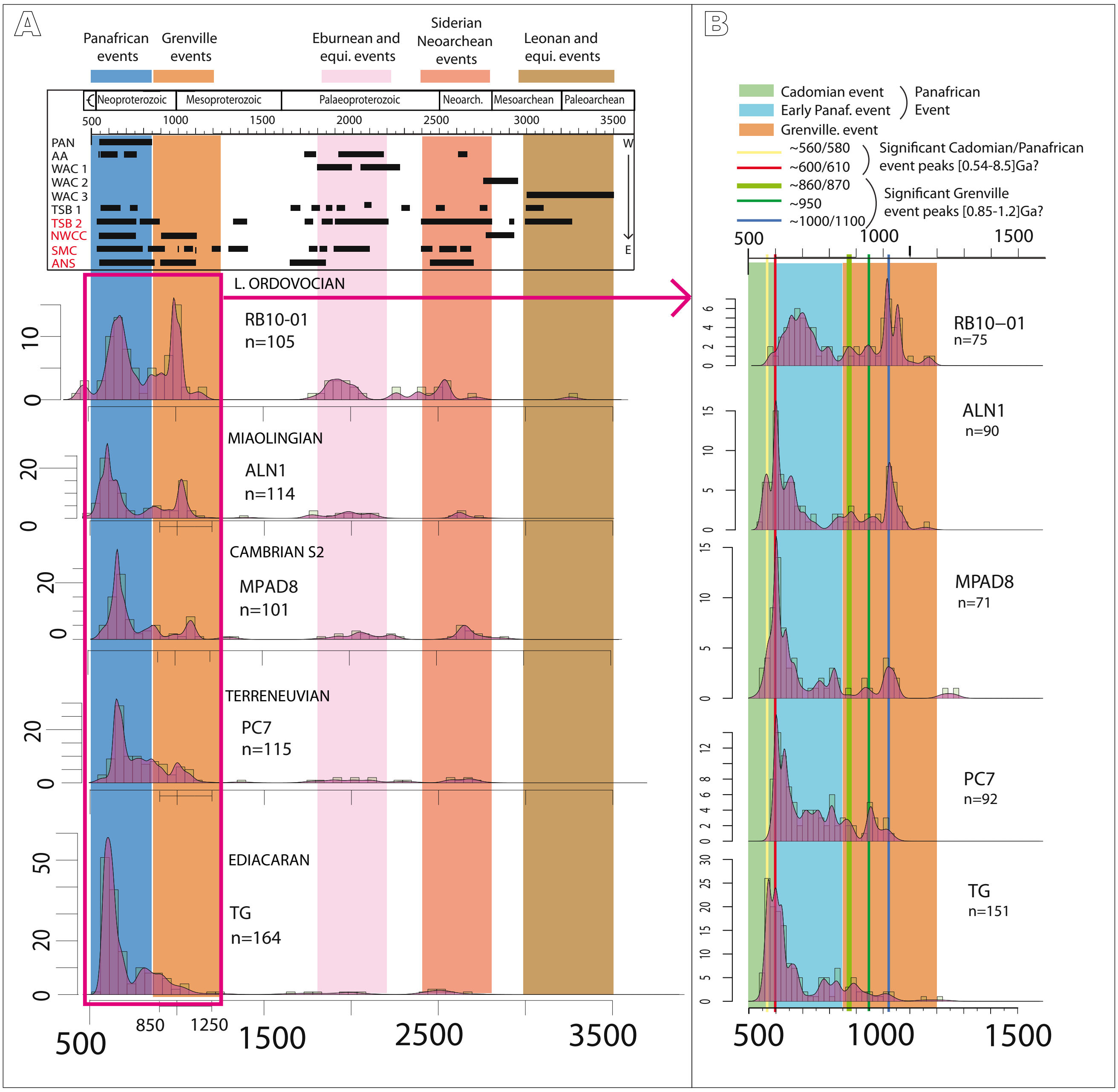


**FIGURE 4.** A) KDE plot for Ediacaran to Lower Ordovician samples from the Pyrenees. The upper part of the diagram shows potential 3500–500Ma zircon sources of detrital zircon populations and potential geological events linked to them. Sources are identified according to the methodology reported by Avigad *et al.* (2003, 2012), Drost *et al.* (2011), Linnemann *et al.* (2011) and Pereira *et al.* (2012). PAN= Panafrican and Cadomian event sources; AA= Anti-Atlasian event sources; WAC1= Eburnean event sources of the West African craton; WAC2= Liberian event sources of the West African craton; WAC3= Leonan event sources of the West African craton; TSB1= Trans-Saharan belt, Benin-Nigerian shield sources; TSB2= Trans-Saharan belt, Tuareg shield sources; SMC= Saharan metacraton; sources ANS= Arabian–Nubian shield sources; NWCC= Northwestern edge of Congo Craton sources. B) KDE plot for zircon populations included in the 1200-450Ma interval illustrating the evolution of some specific peaks through different samples; equo.: equivalent.

U-Pb in situ analysis of single grains were determined at the GeOHeLiS analytical platform (University of Rennes 1) by Laser Ablation Coupled with Plasma source Mass Spectrometry (LA-ICP-MS), using ablation spot diameters of 25$\mu$m, energy pulse of 7J/cm$^{-2}$ and repetition rates of 5Hz. Data were corrected for U-Pb fractionation and for the mass bias by standard bracketing with repeated measurements of the GJ-1 zircon (Jackson *et al.*, 2004). Repeated analyses of the Plešovice zircon standard (Slàma *et al.*, 2008) treated as unknowns were used to control the reproducibility and accuracy of the corrections and yielded a concordia age of 336.7±0.8Ma

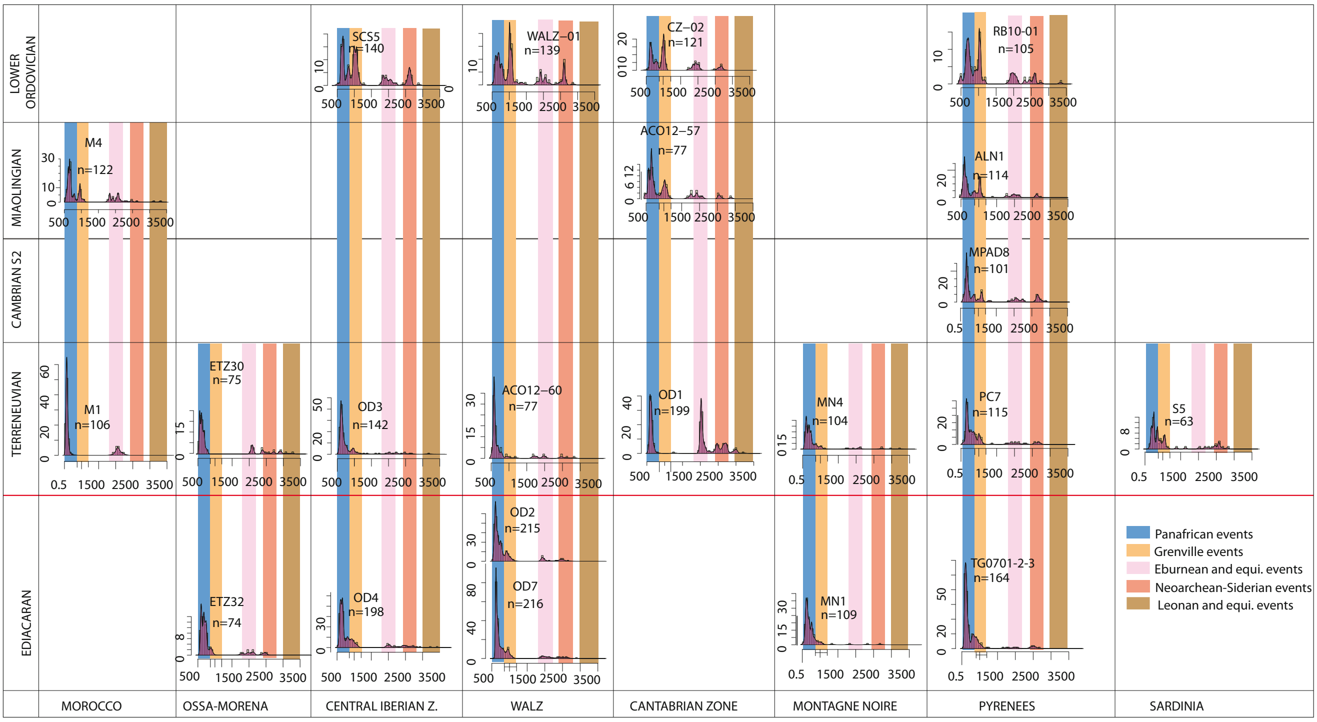


**FIGURE 5.** Comparison of Kernel Density Estimate plot for all samples included in this study.

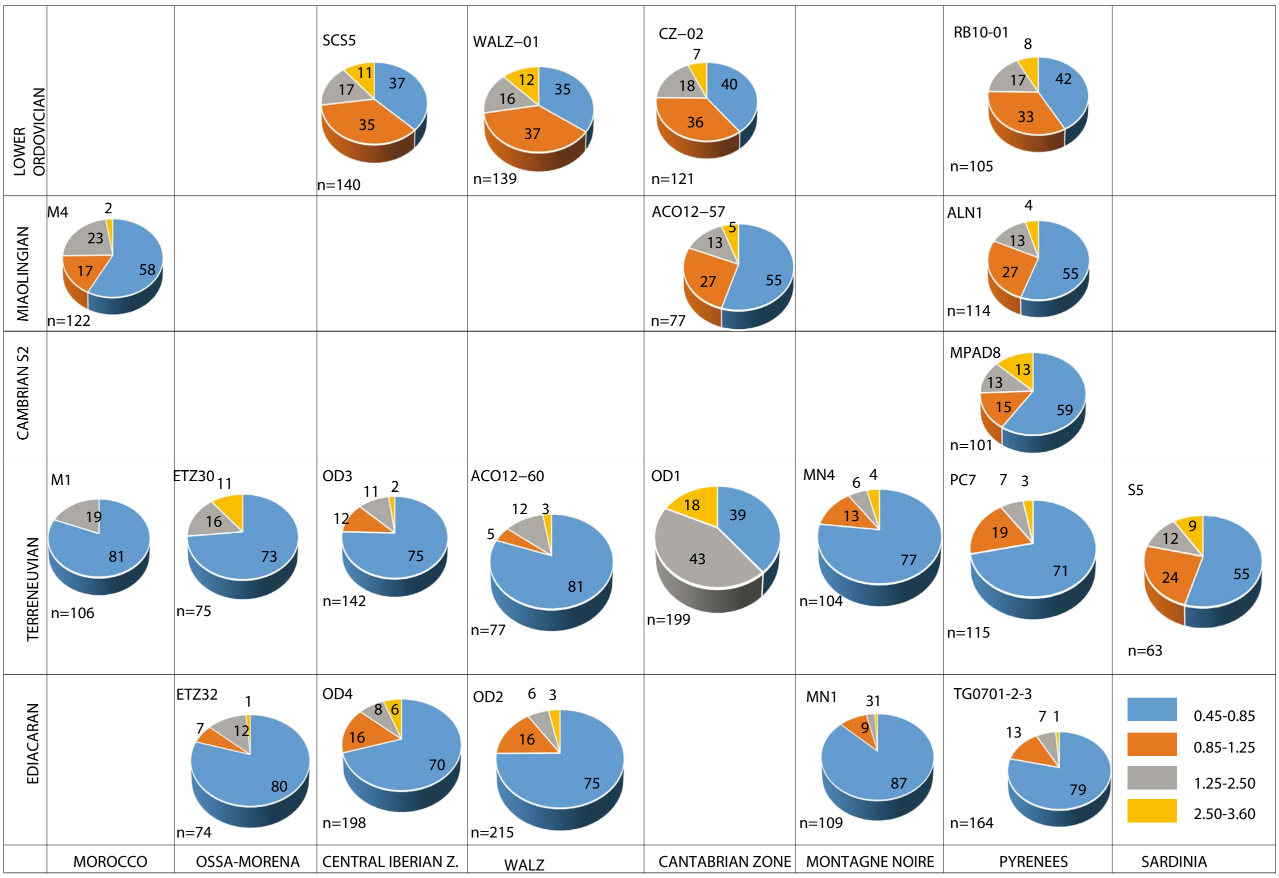


**FIGURE 6.** Pie chart with relative proportion of the different age groups identified in all the samples included in this study.

A — LOWER ORDOVICIAN

| | scs5 | WALZ-01 | CZ-02 | RB10-01 |
|---|---|---|---|---|
| scs5 | | **0.998** | **0.298** | **0.505** |
| WALZ-01 | **0.998** | | **0.302** | **0.480** |
| CZ-02 | **0.298** | **0.302** | | **0.921** |
| RB10-01 | **0.505** | **0.480** | **0.921** | |
| | CIZ | WALZ | Cant. | Pyr. |

K-S P-values using error in the CDF

B — CAMBRIAN MIAOLIGIAN/S2

| | M4 | ACO-12-57 | ALN1 | MPAD8 |
|---|---|---|---|---|
| M4 | | **0.863** | 0.046 | **0.157** |
| ACO-12-57 | **0.863** | | **0.206** | **0.233** |
| ALN1 | 0.046 | **0.206** | | **0.531** |
| MPAD8 | **0.157** | **0.233** | **0.531** | |
| | Moroc. | Cant. | Pyr. | |

K-S P-values using error in the CDF

C — TERRENEUVIAN

| | M1 | ETZ30 | OD3 | ACO-12-60 | OD1 | MN4 | PC7 | S5 |
|---|---|---|---|---|---|---|---|---|
| M1 | | 0.000 | 0.000 | 0.002 | 0.000 | 0.000 | 0.000 | 0.000 |
| ETZ30 | 0.000 | | **0.058** | **0.074** | 0.000 | **0.063** | 0.040 | 0.000 |
| OD3 | 0.000 | **0.058** | | 0.001 | 0.000 | **0.204** | **0.231** | 0.000 |
| ACO-12-60 | 0.002 | **0.074** | 0.001 | | 0.000 | 0.000 | 0.000 | 0.000 |
| OD1 | 0.000 | 0.000 | 0.000 | 0.000 | | 0.000 | 0.000 | 0.000 |
| MN4 | 0.000 | **0.063** | **0.204** | 0.000 | 0.000 | | **0.476** | 0.000 |
| PC7 | 0.000 | 0.040 | **0.231** | 0.000 | 0.000 | **0.476** | | 0.000 |
| S5 | 0.000 | 0.000 | 0.000 | 0.000 | 0.000 | 0.000 | 0.000 | |
| | Moroc. | O-M | CIZ | WALZ | Cant. | Mont. N | Pyr. | Sard. |

K-S P-values using error in the CDF

D — EDIACARAN

| | ETZ32 | OD4 | OD7 | OD2 | MN1 | TG |
|---|---|---|---|---|---|---|
| ETZ32 | | **0.476** | **0.622** | **0.661** | **0.455** | 0.007 |
| OD4 | **0.476** | | 0.029 | **0.860** | 0.041 | 0.007 |
| OD7 | **0.622** | 0.029 | | 0.002 | **0.069** | 0.000 |
| OD2 | **0.661** | **0.860** | 0.002 | | **0.206** | 0.040 |
| MN1 | **0.455** | 0.041 | **0.069** | **0.206** | | **0.099** |
| TG | 0.007 | 0.007 | 0.000 | 0.040 | **0.099** | |
| | O-M | CIZ | WALZ | | Mont. N | Pyr. |

K-S P-values using error in the CDF

**FIGURE 7.** Results of K-S test displayed by all samples. Yellow boxes identify samples with probable identical parent zircon populations with a 95% confidence level. This test has been applied for samples of equivalent age: A) Lower Ordovician, B) Cambrian Miaolingian Series 2, C) Terreneuvian and D) Ediacaran. CIZ= Central Iberian Zone; WALZ= West Asturian-Leonese Zone; Cant= Cantabrian Zone; Pyr= Pyrenees; Moroc= Morocco; O-M= Ossa-Morena; Mont. N= Montagne Noire; Sard= Sardinia.

(n= 36; MSWD= 0.33). Data reduction was carried out with the GLITTER software (Van Achterbergh *et al.*, 2001). More information about the analytical protocol can be found in Manzotti *et al.* (2015), Padel *et al.* (2017a) and in Appendix I.

## U-Pb data treatment: comparison of sources and tectonic settings

All data sets are summarized in Appendix II-IV, where the isotopic ratios and single apparent ages are reported with 1σ errors. In total, 115 grains were analysed from sample PC7, 107 from MPAD8, and 120 from ALN1. In this study, data treatment was made with the analyses that were more than 90% concordant using the $^{207}Pb/^{206}Pb$ apparent ages for zircon older than 1000Ma, and the $^{206}Pb/^{238}U$ apparent ages for the grains that are younger than 1000Ma (Faure and Mensing, 2005; Meinhold *et al.*, 2011; Talavera *et al.*, 2012). The maximum depositional age is calculated using the age of the youngest zircon population from a cluster of at least three concordant analyses from three different grains overlapping in age at 2s (standard deviation), as proposed by Dickinson and Gehrels (2009), to ensure a statistically robust estimate of the maximum depositional ages. As suggested by Manzotti *et al.* (2015), KDE plots (Figs. 4; 5) were built using IsoplotR (Vermeesch, 2018) for sample comparisons with a specific focus on five geological events: the Panafrican, Grenville, Eburnean (or related), Siderian-Neoarchean and Leonan (or related) events. Helped by this graphical proxy, a statistical comparison for equivalent cluster age proportion was made on Neoarchean–Siderian [3.6–2.5Ga], Siderian–Stenian [2.50-1.25Ga], Stenian–Tonian [1.25–0.85Ga] and Tonian-Ediacaran [0.85–0.45Ga] (Fig. 6).

A K-S test was applied to determine if contemporaneous siliciclastic sediments were supplied from similar sources (revealed by a spike on the age distribution) along the NW Gondwana margin (Fig. 7). The K-S test is a non-parametric probabilistic test, useful to compare age distributions from different samples and to discriminate potential statistical differences between them (Guynn and Gehrels, 2010). The test compares the cumulative probability curves, or cumulative distribution functions (CDF), of different zircon populations to evaluate the probability (P) that they might be different (Guynn and Gehrels, 2010). For a K-S test with a 95% confidence level, as used herein, a P-value lower than 0.05 means that the compared populations are significantly different.

Sedimentary basins can be distinguished according to their lithospheric basement, their position with respect to plate boundaries (intracratonic vs. plate margin), and their background plate motion (convergent, collisional, divergent or transform; Allen and Allen, 2005). Cawood *et al.* (2012) introduced a methodology to decipher the type of basin and their relative tectonic settings based on detrital zircon analysis; the authors provided a comparative CA-DA diagram, where the Cumulative Distribution Function (CDF) of zircon age is illustrated based on differences between Crystallization Ages (CA) and Depositional Ages (DA) of the detrital zircon grains. This empirical model considers that convergent settings induce large proportions of detrital zircon crystals with narrow unimodal KDE curves, linked to early magmatic arcs close, in space and time, to the depositional basin (*e.g.* fore-arc, back-arc, intra-arc and foreland cordillera basins). On the contrary, collisional, extensional and intracratonic settings (passive margin, rift and foreland basins) would induce a relatively delayed incorporation of detrital grains characterized by multimodal age distributions (compared to their crystallization age) through possible polyphase reworking. As a result, extensional tectonic settings can be deduced from detrital zircon analyses if CA-DA> 150Ma at 5% of the CDF (step1). If step 1 is not reached, a CA-DA< 100Ma at 30 % of CDF points to a convergent tectonic setting (magmatic arc-related basin; step 2). CA-DA diagrams for Cambrian–Early Ordovician times are used below to analyse variations in sediment sources along Northwest Gondwana. The applicability of this method to decipher the tectonic evolution of the margin is further discussed.

## RESULTS: NEW DATA FROM THE PYRENEAN SAMPLES

In sample PC7 from the Err Formation (Fig. 4), 105 of the 115 analyses are at least 90% concordant. As the depositional age of this sample is Terreneuvian, an age of ~530Ma is selected for the CA-DA diagram (Fig. 9). PC7 displays a predominant Tonian–Cambrian [0.85–0.50Ga] group representing 71% of the data with a second major Stenian–Tonian [1.25–0.85Ga] group around 19% of the grains (Figs. 4; 6), a Siderian–Stenian [2.50–1.25Ga] group (7% of the data), and finally a Palaeoarchean–Neoarchean [3.6–2.5Ga] group representing 3% of the zircon grains. The three youngest concordant and overlapping analysis give a concordant maximum depositional age at 601.9±3.3Ma, MSWD= 1.8 (Appendix V).

In sample MPAD8 from the Serdinya Formation (Fig. 4), 103 of 107 analyses are 90% concordant or more. The depositional age of this sample is dated close to the Cambrian Epoch 2–Miaolingian boundary. Consequently an age of ~514Ma is selected for the CA-DA diagram transition (Fig. 9). In this sample, 59% of the detrital zircons belong to the Tonian–Cambrian [0.85–0.50Ga], 15% are part of a Stenian–Tonian [1.25–0.85Ga] group, while the Siderian–Stenian [2.50–1.25Ga] and Palaeoarchean–Neoarchean [3.6–2.5Ga] groups represent both 13% of the population (Figs. 4; 6). The three youngest concordant and overlapping analysis give a concordant maximum depositional age at 570.2+/-3.0Ma, MSWD= 0.019 (Appendix V).

In sample ALN1 from the Alins/Seo Formation (Fig. 4), 114 of the 120 analyses were at least 90% concordant. The age of this sample is Miaolingian hence an age of ~514Ma is selected for the CA-DA diagram (Fig. 9). In this sample, 55% of the detrital zircons belong to the upper Tonian–Cambrian [0.85–0.50Ga] group, 27 are part of the Stenian–Tonian [1.25–0.85Ga] group, 13% of the Siderian–Stenian [2.50–1.25Ga] group, and 4% of the Palaeoarchean–Neoarchean [3.6–2.5Ga] group (Figs. 4; 6). The three youngest concordant and overlapping analysis give a concordant maximum depositional age at 562.2±3.1Ma, MSWD= 0.57 (Appendix V).

Based on the late Ediacaran to Early Ordovician evolution of the detrital zircon populations from the Pyrenees, a progressive shift from Panafrican-dominant to more diverse sources, including older cratons, can be envisaged. Among these older sources, those related to Grenville events increase from 13% in Ediacaran sedimentary rocks to more than 30% in Ordovician sandstones (Fig. 6), reaching percentages comparable to the Panafrican sources (42%). Two peaks (610–600 and 580–560Ma) are predominant in the Panafrican sources, being the latter peak (580–560Ma) representative of regional Cadomian events (Fig. 4), such as those recorded in the Pic de la Clape ignimbrites (Padel et al., 2018). The 580–560Ma age peak ranges from almost dominant in the Ediacaran samples (TG) to inexistent in the Terreneuvian ones, before their reappearance in Cambrian Epoch 2–Miaolingian samples.

These two peaks disappear in the Early Ordovician samples (Fig. 4), where they are replaced by sources revealing other early Panafrican events. The Grenville sources show two age peaks, which remain stable throughout the Ediacaran to Lower Ordovician samples, where the 1.1–1.0Ga peak progressively increases until becoming the most important of all the Proterozoic sources (Fig. 4). As a result, the oldest sources, poorly represented in Ediacaran samples, progressively become more important as controlled by younger depositional ages arguing for sedimentary input from larger areas, probably involving more open and interconnected basins.

## DISCUSSION

### SW-NE trends in Terreneuvian sedimentary sources

The K-S tests (Fig. 7) characterize the evolution of Ediacaran to Early Ordovician provenance sources along the northwestern Gondwana margin. During the Ediacaran, two ends can be identified: i) a southwesternmost edge where Ossa-Morena shares its zircon pattern with the remaining Iberian Massif, and ii) a northeasternmost edge where the Pyrenees mainly shares its zircon pattern with the Montagne Noire.

During the Terreneuvian, the K-S test shows a possible palaeogeographic constraint with a SW edge (Anti-Atlas), a NE edge (Sardinia), and an intermediate domain (Cantabrian Zone) separating two transects: i) the southwestern Ossa-Morena, Central Iberian and West Asturian-Leonese Zones and ii) the northeastern Montagne Noire and Pyrenees domains (Fig. 7). As a consequence, after comparing zircon populations following a SW-NE-trend, a southwestern source can be recognized mainly feeding the Atlas–Ossa-Morena Rift, a northeastern source feeding the Sardinian margin, and an intermediate area, comprising the Pyrenees, the Montagne Noire and the remaining zones of the Iberian Massif. The effect of the Cantabrian Zone can be explained by a relation between a proximal to distal polarity with other Iberian zones. However, this configuration could also be linked to the presence of a palaeogeographic indentor (Fig. 10) equivalent to the Gondwana promontory model propose by Dias et al. (2016).

Several characteristic Archaean–Palaeoproterozoic zircon populations are identified in all the Terreneuvian–Cambrian Epoch 2 samples. Even if they only represent between 10 to 27% of the global analysed grains, there is a noticeable variation of their relative proportion along NW Gondwana, despite the lack of a distinct pattern probably due to the reduced number of zircon grains. A West African Craton source has often been mentioned to explain the presence of Archaean to Palaeoproterozoic zircon populations in the "lower Cambrian" successions (Avigad et al., 2012 for Morocco and Sardinia; Pereira et al., 2012 for Ossa-Morena Zone; Fernández-Suárez et al., 2014 for the central and northern Iberian Massif zones; Padel et al., 2017 for Montagne Noire). However, the influence of other sources (such as the Arabian Nubian Shield, Saharan Metacraton and Trans-Saharan Belt) cannot be ruled out for most of the studied areas. Although absent in the Terreneuvian–Cambrian Epoch 2 Moroccan sample, Neoarchaean zircon populations (which cannot originate from the West African Craton) are more abundant in other contemporaneous samples. This potentially demonstrates the influence of the Arabian Nubian Shield, the Saharan Metacraton and the Trans-Saharan Belt in the northeastern transect of NW Gondwana. Based on the results yielded by these Terreneuvian–Cambrian Series 2 samples, the Cantabrian Zone seemingly represents an exception with more than 60% of the analysed zircon grains derived from Archaean–Palaeoproterozoic sources. In addition, a significant peak around 2.5Ga and the important influence of Meso– and Mesoarchean sources suggest that the Cantabrian Zone could reflect a central source, such as that of the Trans-Saharan Belt (TSB).

The Amazonian craton has been considered as another potential source for some Palaeo– and Mesoproterozoic zircon crystals sampled in NW Gondwana, or even as the single source for all of them (Fernández-Suárez et al., 2000; Linnemann et al., 2014). The involvement of Amazonian sources was proposed because there were no other ca. 1Ga old sources known in the region at that time (Fernández-Suárez et al., 2014). Since then, such 1Ga old sources have been identified from the Arabian Nubian shield, the Saharan Metacraton, the Trans-Saharan belt (Avigad et al., 2012; Be'eri-Shlevin et al., 2012) and, more recently, from the northwestern edge of the Congo Craton in Cameroun (Bernard et al., 2021). In accordance with Fernández-Suárez et al. (2014), the absence of 1.6–1.2Ga zircon grains in different margins of NW Gondwana can be used as an argument to discard significant sources from the Amazonian craton. Therefore, this craton is not reported in Figures 4 and 10; we consider its influence to be, at best, minimal.

Terreneuvian–Cambrian Series 2 sediments from the Atlas – Ossa-Morena Rift are characterized by a predominant cluster of ca. 0.63–0.54Ga grains, which represent between 81 and 73% of the analyzed zircon populations (Figs. 5; 6). Avigad et al. (2012) proposed a major contribution

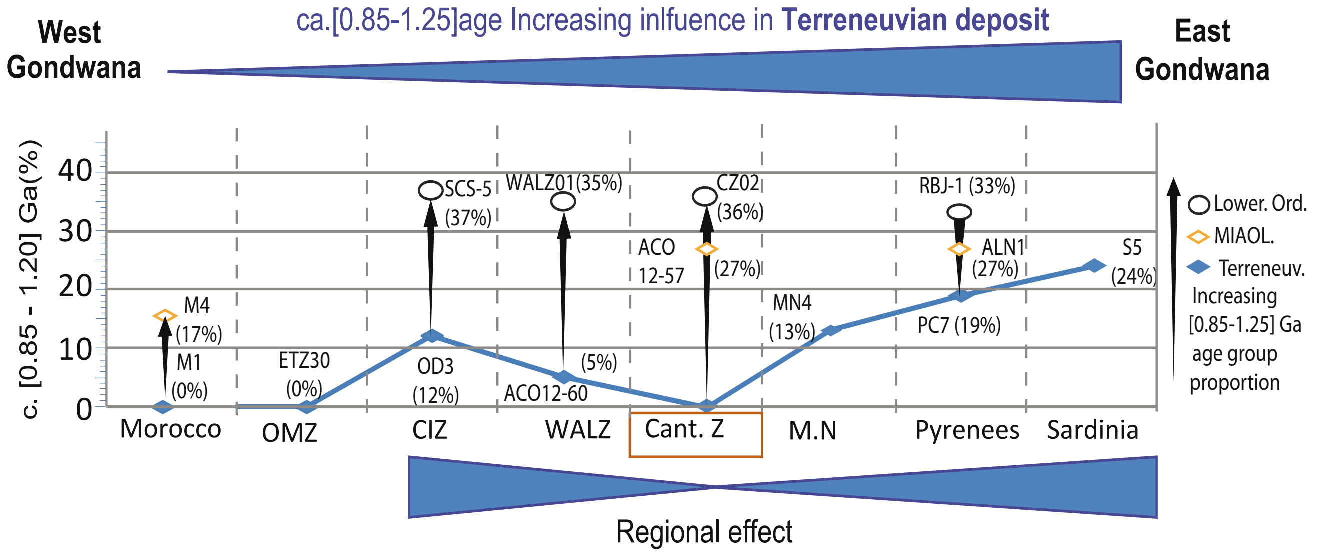


**FIGURE 8.** W-E transect of the northwestern Gondwana margin showing an increasing influence of Stenian–Tonian sources from the Saharan Metacraton and the Arabian-Nubian Shield in Cambro–Ordovician sediments; OMZ= Ossa-Morena Zone; CIZ= Central Iberian Zone; WALZ= West Asturian-Leonese Zone; Cant. Z= Cantabrian Zone; M.N= Montagne Noire

from the upper Ediacaran volcanic event represented by the Ouarzazate Supergroup (the so-called Ediacaran Anti-Atlasian Chain of Pouclet *et al.*, 2008) emplaced during the last stages of the Panafrican orogeny (Álvaro *et al.*, 2014b), and referred below to as the Anti-Atlasian source. Although Pereira *et al.* (2012) suggested that the 0.7–0.54Ga zircon grains from Ossa-Morena (ETZ30) could be derived from the Cadomian arc, the Anti-Atlasian (Blein *et al.*, 2014a, b) and/or TSB sources seem to fit better with the observed ca. 0.63–0.54 age group identified both in the Anti-Atlas and the Ossa-Morena Zone, where older Panafrican zircon crystals (0.95–0.65Ga) are absent or poorly represented. In the two intermediate areas (the Central Iberian and West Asturian-Leonese Zones vs. the Montagne Noire and the Pyrenees), separated by the Cantabrian Zone, 81 to 71% of the analyzed zircon grains form a 0.9–0.5Ga age group (Fig. 6), whereas they represent only 39% in the Cantabrian Zone. For this Panafrican sources, either western (Anti-Atlasian), central (Transsaharian Belt), or eastern (Arabian-Nubian Shield and Saharan Metacraton) sources may be invoked.

Zircon grains related to a 1.25–0.85Ga group (*i.e.* coeval to the Grenville orogeny elsewhere; Figs. 5; 6; 8) are generally associated with the Arabian-Nubian Shield, which was exhumed during Panafrican orogenic events (Caby, 2003; Liégeois *et al.*, 2003; Kroner and Stern, 2005), and/or with the Saharan Metacraton (Avigad *et al.*, 2003; Fernández-Suárez *et al.*, 2014; Shaw *et al.*, 2014; Padel *et al.*, 2017a, b), however, they should also be linked to the northwestern edge of the Congo Craton (Bernard *et al.*, 2021). Such an age group is absent in the "lower Cambrian" siliciclastic strata of the Anti-Atlas and the Ossa-Morena Zone and shows a distinct progressive increase in percentage from the central to the northern Iberian zones (11%) to Sardinia (22%) (Figs. 5; 6; 8). Fernández-Suárez *et al.* (2014) further noticed that sample OD3 (Central Iberian Zone) revealed a zircon age distribution similar to that from "lower Cambrian" samples reported from the northwestern part of the Arabian-Nubian Shield (Israel and Jordan). The influence of both the eastern Arabian-Nubian Shield and the Saharan metacraton increases northeastward along NW Gondwana, where a possible influence of the northwestern edge of the Congo Craton should be also envisaged (Fig. 10).

## Cambrian source evolution and related tectonic settings

Studies of detrital zircon grains yielded by Cambrian Series 2–Lower Ordovician sandstones of Northwest Gondwana are scarce. Only eight samples are available, including four from Cambrian Series 2-Miaolingian and four from Lower Ordovician strata (Figs. 5; 6). Chronological trends in provenance sources are tentatively interpreted based on K-S tests and CA-DA diagrams. According to K-S tests, there are no significant differences between zircon populations (Fig. 7). This supports a relative homogenization of provenance sources along Northwest Gondwana between Cambrian Epoch 2 to Early Ordovician times. The best age group to illustrate this homogenization is the Stenian–Tonian group (Fig. 8), whose proportion, as observed in the Pyrenees, increases from Ediacaran to Lower Ordovician sandstones. The Stenian–Tonian group, associated with sources from the Arabian Nubian Shield, the Saharan Metacraton and the northwestern edge of

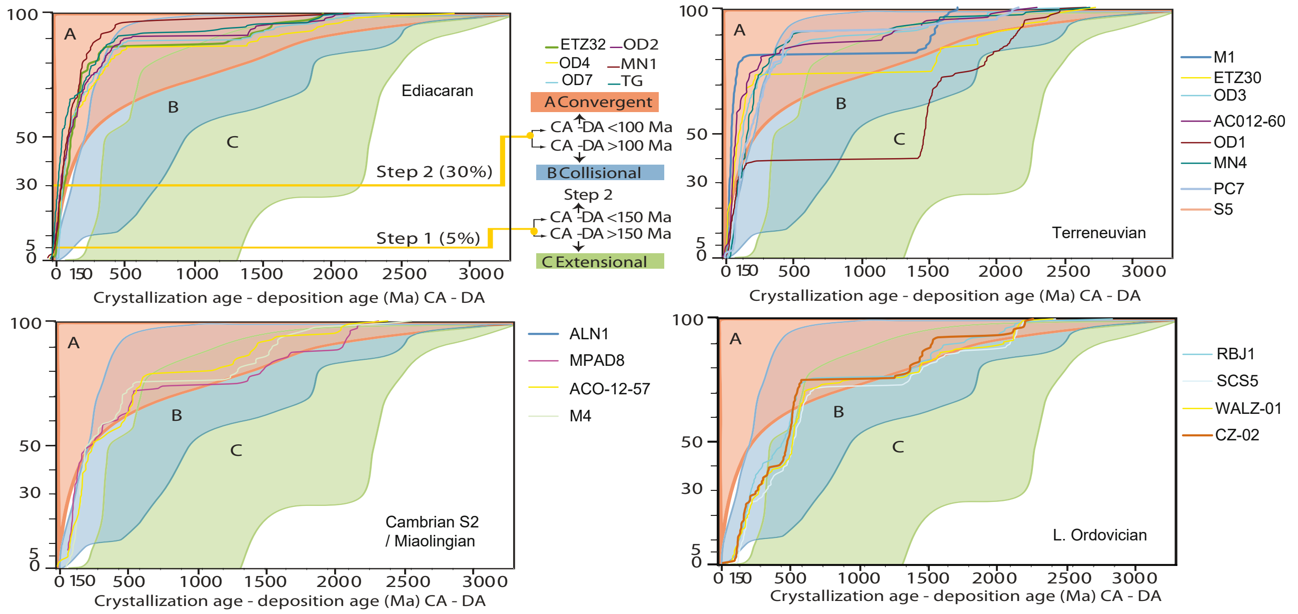


| | Ediacaran | | | | | | Terreneuvian | | | | | | | | Cambrian S2 / Miaolingian | | | | L. Ordovician | | | |
|---|---|---|---|---|---|---|---|---|---|---|---|---|---|---|---|---|---|---|---|---|---|---|
| Samples | ETZ32 | OD4 | OD2 | OD7 | MN1 | TG | M1 | ETZ30 | OD3 | AC012-60 | OD1 | MN4 | PC7 | S5 | M4 | ACO-12-57 | MPAD8 | ALN1 | SCS5 | WALZ-01 | CZ-02 | RB10-01 |
| CA-DA +/- 2σ step 1 | 25±16 | 9±9 | 4±7 | 46±7 | 13±12 | 1±26 | 9±9 | 5±11 | 38±5 | 2±6 | 25±11 | 43±12 | 58±13 | 121±12 | 73±14 | 52±6 | 27±6 | 38±12 | 142±12 | 110±8 | 126±9 | 98±10 |
| CA-DA +/- 2σ step 2 | 80±18 | 66±7 | 60±8 | 72±10 | 66±14 | 38±38 | 30±11 | 60±11 | 87±11 | 51±7 | 86±18 | 91±13 | 100±14 | 207±20 | 150±9 | 152±7 | 98±13 | 98±12 | 335±12 | 287±7 | 264±10 | 229±13 |

**FIGURE 9.** CA-DA diagrams illustrating the interpreted tectonic settings for the reported Terreneuvian–Lower Ordovician samples from Northwestern Gondwana; The table shows the numerical results at the 2 step of the test: an extensional tectonic setting can be deduced from detrital zircon analyses if CA-DA> 150Ma at 5% of the CDF (step1). If step 1 is not reached, a CA-DA< 100Ma at 30% of the CDF points to a convergent tectonic setting (magmatic arc-related basin; step 2), otherwise it could be interpreted as collisional tectonic setting. For abbreviations of samples, see text.

the Congo Craton, which did not influence the Atlas-Ossa-Morena Rift during the Terreneuvian, subsequently provided up to 16% of the inherited grains during the Miaolingian (Fig. 8). A comparison of isotopic Hf values in the Stenian-age population of zircons from Morocco and Sardinia, Avigad *et al.* (2012) suggested two distinct Stenian sources feeding the western and eastern edges of NW Gondwana. Figure 8 illustrates the evolution of this specific age group. During Terreneuvian times, the 1.25–0.85Ga age group suggests that the Pyrenees would be located between Montagne Noire and Sardinia. In the Cantabrian Zone, the 1.25–0.85Ga age group is not well-represented in the zircon population of sample OD1 (Fig. 8). In addition, the K/S test shows that OD1 appears to be significantly different from other Terreneuvian samples of the intermediate zone. These results suggest that, during the Terreneuvian, the Cantabrian margin was distinctive enough to represent the hinge of the southwestern and a northeastern transects. The evolution of this age group during the Ediacaran–Terreneuvian interval displays two distinct behaviours: the western Ossa-Morena and West Asturian-Leonese Zones transect is characterized by a lower proportion of the 1.25–0.85Ga group, whereas this age group is characterized by a progressive increase in the eastern Montagne Noire and Pyrenees transect (Figs. 5; 6; 8). Although the early Palaeozoic palaeogeographic position of the Pyrenean margin cannot be definitely assessed, the analysis of this 1.25–0.85Ga age group suggests a strong affinity with the Montagne Noire and Sardinia, probably standing between them (Álvaro *et al.*, 2021).

At the end of Terreneuvian times, the above-reported SW-NE trend is interpreted to reflect a delayed shift in tectonic activity. The amalgamation of the Gondwana supercontinent (Stern, 1994; Ballèvre *et al.*, 2001; Meert, 2003; Kroner and Stern, 2005; Stampfi and von Raumer, 2008; Murphy *et al.*, 2013; Stampfi *et al.*, 2013; Linnemann *et al.*, 2014; Blein *et al.*, 2014a, b) is recorded in the studied area by the Panafrican and Cadomian orogens, which ended up close to the Ediacaran–Cambrian time interval. During the early Palaeozoic, the geodynamic setting of Northwest Gondwana changed drastically from convergent to extensional, marking the beginning of an interconnected rifting phase that ended with the opening of the Rheic Ocean (Ballèvre *et al.*, 2001; Linnemann *et al.*, 2007, 2008; Pereira *et al.* 2012; Stampfi *et al.*, 2013; Pouclet *et al.*, 2017).

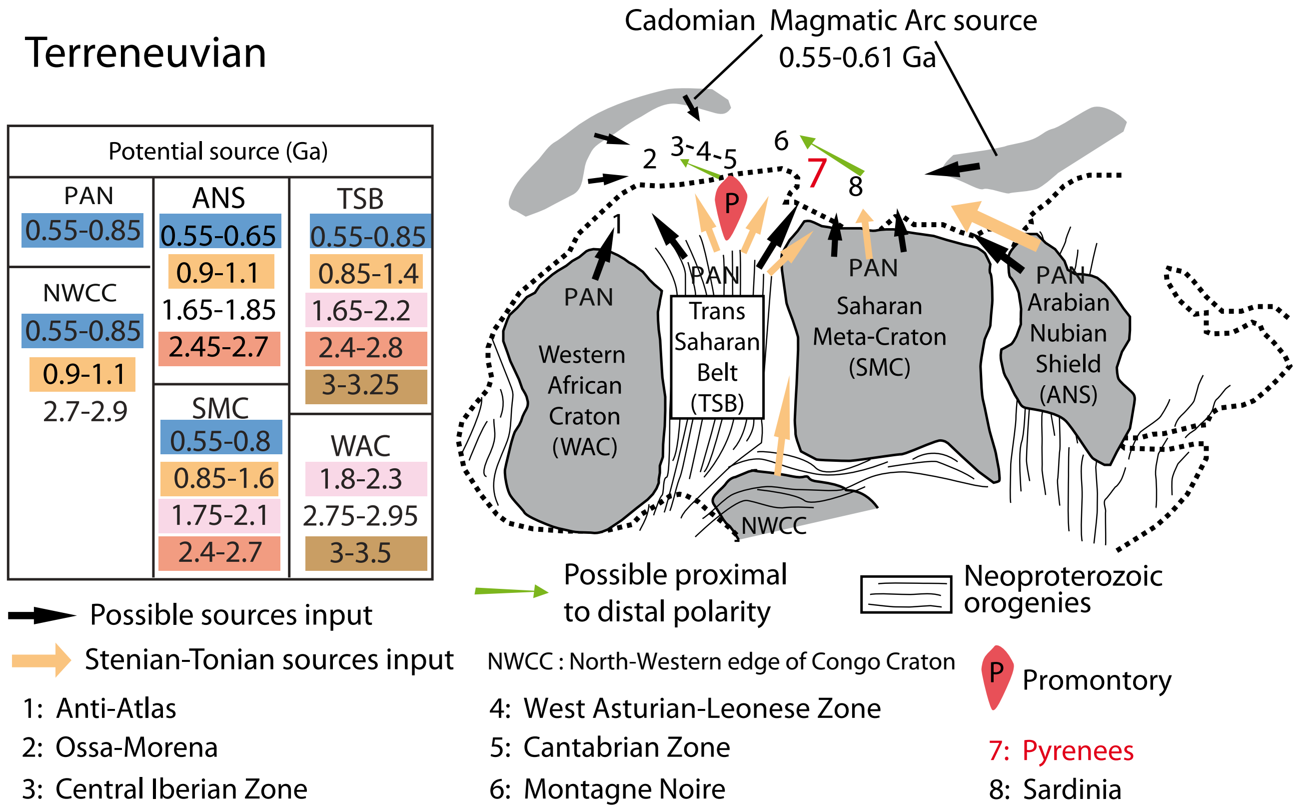


**FIGURE 10.** Tentative palaeoposition reconstruction of the different peri-Gondwana transects reported in the text according to the influence of their zircon supply potential sources. The promontory (P in the figure) is proposed as an effect of the Cantabrian Zone which be link to the presence of an indentation equivalent to the Gondwana promontory proposed, among others, by Dias *et al.* (2016).

The arc/rift/drift evolution is not clearly reflected by the CA-DA diagram (Fig. 9). Data from the Ediacaran samples fit well with a convergent setting. The Terreneuvian sandstones from the Anti-Atlas (M1), Ossa-Morena (ETZ30), Central Iberian (OD3), West Asturian-Leonese (ACo12-60), Cantabrian (OD1) Zones and the Montagne Noire (MN4) plot in the CA-DA diagram within the convergent field (A field in Fig. 9), while the remaining samples plot within the collisional field (B field in Fig. 9). These results disagree with other geological evidences, which rather support an extensional regime with the onset of rifting conditions along the margin (Linnemann *et al.*, 2007, 2008; Stampfi and von Raumer, 2008; Álvaro *et al.*, 2016, 2021; Pouclet *et al.*, 2017). However, this apparent mismatch between the CA-DA model and the geological evidence can be linked to two major factors that controlled the zircon populations deposited in an early extensional setting, which are not integrated in the CA-DA model: i) the time-laps since the last convergent setting (as illustrated, for example, by Cawood *et al.*, 2012 for Furongian deposits from Avalonia) and ii) the distance between the sources and the setting of deposition. The effects on the CA-DA diagram, known as the "closeness of a recent source", and its interpretation are well illustrated in the studied "lower Cambrian" samples.

The fast post–Panafrican and post–Cadomian shift from convergent to extensional conditions, and the short distances between the settings of deposition and the major Ediacaran Panafrican and Anti-Atlasian sources, explain their permanent influence in Terreneuvian sediments of the Atlas (M1)–Ossa-Morena (ETZ30) Rift, as illustrated by the major peak in zircon age distributions and the reduced CA-DA values. The influence of these sources subsequently vanished, resulting in a more flattened and equilibrated age distribution, with a more balanced influence of relatively distant sources of various ages, and higher CA-DA values. In our case study, the easternmost edge (Pyrenees and Sardinia) is rather distant from any source inherited from the late Meso– to Neoproterozoic orogens, such as the Panafrican or Anti-Atlasian ones (located to the Southwest), or the Arabian-Nubian Shield and Sahara metacraton (to the Northeast). Hence the Pyrenees and Sardinia display a more balanced distribution of zircon composition, increasing their relative CA-DA values, which could explain their "apparent" misleading position in the collisional field. From Cambrian Epoch 2 to Miaolingian times, the effect of the closeness to recent sources progressively decreased. In the present case, the different major Meso– to Neoproterozoic sources tend to enlarge their target to more distant basins, again stretching the zircon age curve repartition and increasing the CA-DA value in siliciclastic successions (M4, ACO12-57, MPAD8, ALN1). Only the Lower Ordovician sandstones of the Central-Iberian Zone (SCS5, within error), deposited in "post-transitional" extensional settings (Shaw *et al.*, 2014; Margalef *et al.*, 2016; Pouclet *et al.*, 2017) and reflect a CA-DA particularity significative (CA-DA at step 1= 142±12Ma; Fig. 9).

Nonetheless, both the KDE and CA-DA diagrams for Terreneuvian successions suggest an eastward decreasing influence of the Panafrican and/or Anti-Atlasian sources, together with an increase in the influence of the Meso– to Neoproterozoic Arabian-Nubian Shield and Sahara sources, in a context of relatively rapid transition from convergent to extensional settings. The KDE and CA-DA diagrams also suggest a rapid change in geodynamic conditions from a Terreneuvian post-collisional phase, evolving to extensive dynamics that stabilised in the Furongian–Early Ordovician. The end of rifting conditions or rift-drift turnover led to the establishment of a passive margin that also affected the Occitan and South Armorican domains during early Ordovician times (Pouclet *et al.*, 2017)

Additional biogeographic links and distinct magmatic episodes support the palaeogeographic interpretations based on zircon population sources. The patch-reefs sampled in the Terrades inlier of the eastern Pyrenees have recently provided a rich fossil record comprising archaeocyaths, bradoriids, brachiopods, molluscs, tommotiids, chancelloriids, hyoliths and problematic microfossils (Perejón *et al.*, 1994; Wallet *et al.*, 2021), with strong biogeographic links with both the Montagne Noire and Sardinia. The Pyrenees also share with the Montagne Noire and Sardinia: i) the presence of late Ediacaran–early Terreneuvian felsic explosive calc-alkaline tuffs related to the Cadomian orogen, despite the absence of Cadomian metamorphic events (Álvaro *et al.*, 2014a; Padel *et al.*, 2017a, b, 2018); ii) a carbonate production across the Cambrian Series 2-Miaolingian transition; iii) the lack of the Furongian–Early Ordovician Toledanian Phase, associated with the onset of a break-up unconformity; and iv) a distinct record of the Mid–Ordovician Sardic Phase reflecting thermal doming, generalized denudation of areas uplifted under subaerial conditions, and intrusion of massive peraluminous granitic bodies (Álvaro *et al.*, 2016, 2021). All these complementary observations suggest that the Cambrian Pyrenean margin was probably located between the Cantabrian-Montagne Noire and the Sardinian margins of West Gondwana (Figs. 8; 10).

## CONCLUSIONS

Detrital zircon grains from Ediacaran–Lower Ordovician sandstones and quartzites sampled in the Pyrenees were dated by LA-ICPMS in order to assess their provenance sources. The resulting age distributions are compared to other available datasets from neighbouring margins, such as Morocco, the Iberian Peninsula, France and Sardinia. K-S test, KDE and CA-DA diagrams were used to compare zircon populations estimating their possible correlation with the arc/rift/drift geodynamic evolution recorded in Northwest Gondwana.

During Terreneuvian times, three areas can be distinguished: a southwestern edge (comprising the Atlas-Ossa-Morena Rift), a central transitional area (encompassing the central and northern Iberian Massif Zones, the Montagne Noire and the Pyrenees), and a northeastern edge (Sardinia). The relative influence of major sediment sources follows a SW–NE trend. Indeed, the Panafrican-Anti-Atlasian sources predominate within the southwesternmost successions, whereas the influence of the Arabian-Nubian Shield and Sahara Metacraton sources increases northeastward. The Terreneuvian trend gradually disappeared throughout Cambrian Epoch 2 to Early Ordovician times. This pattern reflects the evolution of geodynamic settings along NW Gondwana, with a rapid post–Panafrican shift to rifting and drifting conditions. Although the palaeogeographic position of the Pyrenean margin cannot be definitely assessed, the analysis of zircon populations from Cambro–Ordovician strata supports former biogeographic, stratigraphic and magmatic studies, suggesting a strong affinity with the Montagne Noire and Sardinia domains, tentatively locating the Pyrenees between both margin transects.

## ACKNOWLEDGMENTS

This research was founded by the RGF program of the French Geological Survey (BRGM). This paper is a contribution to project CGL2013-48877-P from Spanish MINECO. François Guillot, Olivier Blein, Cecilio Quesada and Cesar Witt are warmly thanked for stimulating discussions about Cadomian geodynamics. The authors appreciate revisions by Noel Moreira (Evora, Portugal) and an anonymous reviewer.

## REFERENCES

Allen, P.A., Allen, J.R., 2005. Basin Analysis. Principles and Applications. Cambridge, Blackwell Scientific Publications, 562pp.

Altumi, M.M., Elicki, O., Linnemann, U., Hofmann, M., Sagawe, A., Gärtner, A., 2013. U-Pb LA-ICP-MS detrital zircon ages from the Cambrian of Al Qarqaf Arch, central-western Libya: provenance of the West Gondwanan sand sea at the dawn of the early Palaeozoic. Journal of African Earth Sciences, 79, 74–97.

Álvaro, J.J., Bauluz, B., Clausen, S., Devaere, L., Imaz, A.G., Monceret, E., Vizcaïno, D., 2014a. Stratigraphy of the Cambrian–Lower Ordovician volcanosedimentary complexes in the northern Montagne Noire, France. Stratigraphy, 11, 83–96.

Álvaro, J.J., Benziane, F., Thomas, R., Walsh, G.J., Yazidi, A., 2014b. Neoproterozoic–Cambrian stratigraphic framework of the Anti-Atlas and the Ouzellagh promontory (High Atlas), Morocco. Journal of African Earth Sciences, 98, 1–15.

Álvaro, J.J., Colmenar, J., Monceret, E., Pouclet, A., Vizcaïno, D., 2016. Late Ordovician (post–Sardic) rifting branches in the North Gondwanan Montagne Noire and Mouthoumet massifs of southern France. Tectonophysics, 681, 111–123.

Álvaro, J.J., Sánchez-García, T., Puddu, C., Casas, J.M., Díez-Montes, A., Liesa, M., Oggiano, G., 2020. Comparative geochemical study on Furongian–earliest Ordovician (Toledanian) and Ordovician (Sardic) felsic magmatic events in south-western Europe: underplating of hot mafic magmas linked to the opening of the Rheic Ocean. Solid Earth, 11, 2377–2409.

Álvaro, J.J., Casas, J.M., Quesada, C., 2021. Reconstructing the pre–Variscan puzzle of Cambro–Ordovician basement rocks in the southwestern European margin of Gondwana. In: Murphy, J.B., Strachan, R.A., Quesada, C. (eds.). Pannotia to Pangaea: Neoproterozoic and Paleozoic Orogenic Cycles in the Circum-Atlantic Region. Geological Society, London, Special Publications 503, 531–562

Avigad, D., Kolodner, K., McWillians, M., Persing, H., Weissbroad, T., 2003. Origin of northern Gondwana Cambrian sandstone revealed by detrital zircon SHRIMP. Geology, 31, 227-230.

Avigad, D., Gerde, A., Morag, N., Bechstädt, T., 2012. Coupled U-Pb-Hf of detrital zircons of Cambrian sandstones from Morocco and Sardinia: implications for provenance and Precambrian crustal evolution of North Africa. Gondwana Research, 21, 690–703.

Avigad, D., Rossi, Ph., Gerdes, A., Abdo, A., 2018. Cadomian metasediments and Ordovician sandstone from Corsica: detrital zircon U-Pb-Hf constrains on their provenance and paleogeography. International Journal of Earth Sciences, 107, 2803–2818.

Ballèvre, M., Le Goff, E., Hébert, R., 2001. The tectonothermal evolution of the Cadomian belt of northern Britany, France: a Neoproterozoic volcanic arc. Tectonophysics, 331, 19–43.

Ballèvre, M., Bosse, V., Ducassou, C., Pitra, P., 2009. Palaeozoic history of the Armorican Massif: models for the tectonic evolution of the suture zones. Comptes Rendus Geoscience, 341, 174–201.

Ballouard, C., Poujol, M., Zeh, A., 2018. Multiple crust reworking in the French Armorican Variscan belt: implication for the genesis of uranium-fertile leucogranites. International Journal of Earth Sciences,107, 2317–2336.

Barnolas, A., Chiron, J.C., 1996. Synthèse géologique et géophysique des Pyrénées. Tome 1: Cycle hercynien. Orléans-Madrid, Bureau de Recherche Géologique et Minière – Instituto Tecnológico y Geominero de España, 729pp.

Be'eri-Shlevin, Y., Eyal, M., Eyal, Y., Whitehouse, M.J., Livinovsky, B., 2012. The Sa'al volcano-sedimentary complex (Sinai, Egypt): a latest Mesoproterozoic volcanic arc in the northern Arabian Nubian Shield. Geology, 40, 403–406.

Bernard, J., Couëffé, R., Blein, O., Vic, G., Buscail, F., Tchokona Seuwui, D., Wongolo Djombol, M.H., Tucker, R., Cagnard, F., Duron, J., Martelet, G., Bailly, L., Chevillard, M., Colin, S., Chabot, L., Gutierrez, T., Lahaye, Y., Anaba Fotze, Q.M., Eno-Tabi Lobe Makia, G., Ndapeh Ndellejong, B., Essomba, Y.H., 2021, Carte géologique du Cameroun à 1/200 000 – Feuilles Batouri (NB-33-III), Betare-Oya (NB-33-IX), Meiganga (NB-33-XV), Belel (NB-33-XXI), Rey-Bouba (NC-33-III). Ministère des Mines, de l'Industrie et du Développement technologique du Cameroun, Yaoundé, Notice explicative, 224pp.

Blein, O., Baudin, T., Soulaimani, A., Cocherie, A., Chèvremont, P., Admou, H., Ouanaimi, H., Hafid, A., Razin, P., Bouadbelli, M., Roger, J., 2014a. New geochemical, geochronological and structural constraints on the Ediacaran evolution of the south Sirwa, Agadir-Melloul and Iguerda inliers, Anti-Atlas, Morocco. Journal of African Earth Sciences, 98, 47–71.

Blein, O., Baudin, T., Chèvremont, Ph., Soulaimani, A., Admou, H., Gasquet, D., Cocherie, A., Egal, E., Youbi, N., Razin, Ph., Bouabdelli, M., Gombert, Ph., 2014b. Geochronological constraints on the polycyclic magmatism in the Bou Azzer-El Graara inlier (Anti-Atlas, Morocco). Journal of African Earth Sciences, 99, 287–306.

Caby, R., 2003. Terrane assembly and geodynamic evolution of central-western Hoggar: a synthesis. Journal of African Earth Sciences, 37, 133–159.

Casas, J.M., Murphy, J.B., 2018. Unfolding the arc: the use of pre-orogenic constraints to assess the evolution of the Variscan belt in Western Europe. Tectonophysics, 736, 47–61.

Cass, J.M., Palacios, T., 2012. First biostratigraphical constraints on the pre–Upper Ordovicians sequences of the Pyrenees based on organic-walled microfossils. Comptes Rendus Geoscience, 344, 50–56.

Casas, J.M., Castiñeiras, P., Navidad, M., Liesa, M., Carreras, J., 2010. New insights into the Late Ordovician magmatism in the Eastern Pyrenees: U-Pb SHRIMP zircon data from the Canigó massif. Gondwana Research, 17, 317–324.

Casas, J.M., Navidad, M., Castiñeiras, P., Liesa, M., Aguilar, C., Carreras, J., Hofman, M., Gärtner, A., Linnemann, U., 2015. The Late Neoproterozoic magmatism in the Ediacaran series of the Eastern Pyrenees: new ages and isotope geochemistry. International Journal of Earth Sciences, 104, 909–925.

Castiñeiras, P., Navidad, M., Liesa, M., Carreras, J., Casas, J.M., 2008. U-Pb zircon ages (SHRIMP) for Cadomian and Lower Ordovician magmatism in the Eastern Pyrenees: new insights in the pre–Variscan evolution of the northern Gondwana margin. Tectonophysics, 46, 228–239.

Cawood, P.A., Hawkesworth, C.J., Dhuime, B., 2012. Detrital zircon record and tectonic setting. Geology, 40, 875–878.

Cochelin, B., Lemirre, B., Denèle, Y., De Saint Blanquat, M., Lahfid, A., Duchêne, S., 2018. Structural inheritance in the

Central Pyrenees: the Variscan to Alpine tectonometamorphic evolution of the Axial Zone. Journal of the Geological Society, 175, 336–351.

Cocherie, A., Baudin, T., Autran, A., Guerrot, C., Fanning, M., Laumonier, B., 2005. U-Pb zircon (ID-TIMS and SHRIMP) evidence for the early Ordovician intrusion of metagranites in the late Proterozoic Canaveilles Group of the Pyrenees and the Montagne Noire (France). Bulletin de la Société géologique de France, 176, 269–282.

Couzinié, S., Laurent, O., Chelle-michou, C., Bouilhol, P., Paquette, J.L., Gannoun, A.M., Moyen, J.F., 2019. Detrital zircon U-Pb-Hf systematics of Ediacaran metasediments from the French Massif Central: consequences for the crustal evolution of the north Gondwana margin. Precambrian Research, 324, 269–284.

Deloule, E., Alexandrov, P., Cheilletz, A., Laumonier, B., Barbey, P., 2002. In situ U-Pb zircon ages for Early Ordovician magmatism in the eastern Pyrenees, France: the Canigou orthogneisses. International Journal of Earth Sciences, 91, 398–405.

Denèle Denèle, Y., Barbey, P., Deloule, E., Pelleter, E., Olivier, Ph., Gleizes, G., 2009. Middle Ordovician U-Pb age of the Aston and Hospitalet orthogneissic laccoliths: their role in the Variscan evolution of the Pyrenees. Bulletin de la Société géologique de France, 180(3), 209–216.

Dias, R., Ribeiro, A., Romão, J., Coke, C., Moreira, N., 2016. A review of the arcuate structures in the Iberian Variscides; constraints and genetic models. Tectonophysics, 681, 170–194.

Dickinson, W.R., Gehrels, G.E., 2009. Use of U–Pb ages of detrital zircons to infer maximum depositional ages of strata: a test against a Colorado Plateau Mesozoic database. Earth and Planetary Science Letters, 288, 115–125.

Drost, K., Gerdes, A., Jeffries, T., Linnemann, U., Storey, C., 2011. Provenance of Neoproterozoic and early Paleozoic silicicastic rocks of the Tepla-Barrandian unit (Bohemian Massif): evidence from U-Pb detrital zircon ages. Gondwana Research, 19, 213–231.

Faure, G., Mensing, T.M., 2005. Isotopes: principles and applications. Wiley, Hoboken, 928pp.

Fernández-Suárez, J., Gutiérrez-Alonso, G., Jenner, G.A., Tubrett, M.N., 2000. New ideas on the Proterozoic–Early Palaeozoic evolution of NW Iberia: insights from U-Pb detrital zircon ages. Precambrian Research, 102, 185–206.

Fernández-Suárez, J., Gutiérrez-Alonso, G., Pastor-Galán, D., Hofmann, M., Murphy, J.B., Linnemann, U., 2014. The Ediacaran–Early Cambrian detrital zircon record of NW Iberia: possible sources and paleogeographic constraints. International Journal of Earth Sciences, 103, 1335–1357.

Gehrels, G., 2014. Detrital zircon U-Pb geochronology applied to tectonics. Annual Review of Earth and Planetary Sciences, 42, 127–149.

Gutiérrez-Alonso, G., Fernández-Suarez, J., Jeffries, T.E., Jenner, G.A., Tubrett, M.N., Cox, R., Jackson, S.E., 2003. Terrane accretion and dispersal in the northern Gondwana margin. An Early Paleozoic analogue of a long-lived active margin. Tectonophysics, 365, 221–232.

Gutiérrez-Alonso, G., Fernández-Suarez, J., Pastor-Galán, D., Johnston, S.T., Linnemann, U., Hofmann, M., Shaw, J., Colmenero, J.R., Hernández, P., 2015. Significance of detrital zircons in Siluro–Devonian rocks from Iberia. Journal of the Geological Society, 172, 309–322.

Guynn, J., Gehrels, G., 2010. Comparison of detrital zircon age distributions using the K-S test. Last accessed: April 2010 Website: https://sites.google.com/a/laserchron.org/laserchron/

Henderson, B.J., Collins, W.J., Murphy, J.B., Gutiérrez-Alonso, G., Hand, M., 2016, Gondwanan basement terranes of the Variscan–Appalachian orogeny: Baltican, Saharan and West African hafnium isotopes fingerprints in Avalonia, Iberia and the Armorican Terranes. Tectonophysics, 681, 278–304.

Jackson, S.E., Pearson, N.J., Griffin, W.L., Belousova, E.A., 2004. The application of laser-ablation-inductively coupled plasma-mass spectrometry to in situ U-Pb zircon geochronology. Chemical Geology, 211, 47–69.

Kroner, A., Stern, R.J., 2005. Pan-African orogeny. Encyclopedia of Geology, 1, 1–12.

Kydonakis, K., Kostopoulos, D., Poujol, M., Brun, J.P., Papanikolaou, D., Paquette, J.L., 2014. The dispersal of the Gondwana super-fan system in the eastern Mediterranean: new insights from detrital zircon geochronology. Gondwana Research, 25, 1230–1241.

Laumonier, B., Abad, A., Alonso, J.L., Baudelot, S., Bessière, G., Besson, M., Bouquet, C., Bourrouilh, R., Brula, P., Carreras, J., Centène, A., Courjault-Radé, R., Courtessole, R., Fauconnier, D., García-Sansegundo, J., Guitard, G., Moreno-Eiris, E., Perejón, A., Vizcaïno, D., 1996. Cambro–Ordovicien. In: Barnolas, A., Chiron, J.C. (eds.). Synthèse géologique et géophysique des Pyrénées. Tome 1: Cycle hercynien. Orléans-Madrid, Bureau de Recherche Géologique et Minière – Instituto Tecnológico y Geominero de España, 729pp.

Laumonier, B., Autran, A., Barbey, P., Cheilletz, A., Baudin, T., Cocherie, A., Guerrot, C., 2004. Conséquences de l'absence de socle cadomien sur l'âge et la signification des séries pré–varisques (anté–Ordovicien supérieur) du sud de la France (Pyrénées, Montagne Noire). Bulletin de la Société géologique de France, 175, 105–117.

Laumonier, B., Calvet, M., Wiazemsky, M., Barbey, P., Marignac, C., Lambert, J., Lenoble, J.L., 2015. Notice explicative de la Carte géologique de la France (1/50.000), feuille Céret (1096). Bureau de Rercherche Géologique et Minière, Orléans.

Lemirre, B., Cochelin, B., Duchene, S., de Saint Blanquat, M., Poujol, M., 2019. Origin and duration of late orogenic magmatism in the foreland of the Variscan belt (Lesponne - Chiroulet - Neouvielle area, French Pyrenees). Lithos, 336, 183–201.

Liégeois, J.P., Latouche, L., Boughara, M., Navez, J., Guiraud, M., 2003. The LATEA metacraton (Central Hoggar, Tuareg Shield, Algeria): behaviour of an old passive margin during the Pan-African orogeny. Journal of African Earth Sciences, 37, 161–190.

Liesa, M., Carreras, J., Castiñeiras, P., Casas, J.M., Navidad, M., Vila, M., 2011. U-Pb zircon of Ordovician magmatism in the Albera Massif (Eastern Pyrenees). Geologica Acta, 9(1), 93–101.

Linnemann, U., Gerdes, A., Drost, K., Buschmann, B., 2007. The continuum between Cadomian Orogenesis and opening of the Rheic Ocean: constraints from LA-ICP-MS U-Pb zircon dating and analysis of plate-tectonic setting (Saxo-Thuringian Zone, NE Bohemian massif, Germany). In: Linnemann, U., Nance, D., Kraft, P., Zulauf, G. (eds.). The Evolution of the Rheic Ocean: from Avalonian–Cadomian Active Margin to Alleghenian–Variscan Collision. Geological Society of America, 423 (Special Papers), 423, 61–96.

Linnemann, U., Pereira, F., Jeffries, T.E., Drost, K., Gerdes, A., 2008. The Cadomian Orogeny and the opening of the Rheic Ocean: the diacrony of geotectonic processes constrained by LA-ICP-MS U-Pb zircon dating (Ossa-Morena and Saxo-Thuringian Zones, Iberian and Bohemian Massifs). Tectonophysics, 461, 21–43.

Linnemann, U., Ouzegane, K., Drareni, A., Hofmann, M., Becker, S., Gärtner, A., Sagawe, A., 2011. Sands of West Gondwana: an archive of secular magmatism and plate interactions – a case study from the Cambro–Ordovician section of the Tassili Ouan Ahaggar (Algerian Sahara) using U–Pb LA-ICP-MS detrital zircon ages. Lithos, 123, 188–203.

Linnemann, U., Gerdes, A., Hofmann, M., Marko, L., 2014. The Cadomian Orogen: Neoproterozoic to Early Cambrian crustal growth and orogenic zoning along the periphery of the West African Craton – Constraints from U-Pb zircon ages and Hf isotopes (Schwarzburg Antiform, Germany). Precambrian Research, 244, 236–278.

Manzotti, P., Poujol, M., Ballèvre, M., 2015. Detrital zircon in blueschist-facies metaconglomerates: implications for the Early Permian palaeo-topography of the Western Alps. International Journal of Earth Sciences, 104, 703–731.

Margalef, A., Castiñeiras, P., Casas, J.M., Navidad, M., Montserrat, L., Linnemann, U., Hofmann, M., Gärtner, A., 2016. Detrital zircons from the Ordovician rocks of the Pyrenees: geochronological constraints and provenance. Tectonophysics, 681, 124–134.

Martínez, F.J., Iriondo, A., Dietsch, C., Aleinikoff, J.N., Peucat, J.J., Cirès, J., Reche, J., Capdevila, R., 2011. U-Pb SHRIMP-RG zircon ages and Nd signature of lower Paleozoic rifting-related magmatism in the Variscan basement of the Eastern Pyrenees. Lithos, 127, 10–23.

Martínez Catalán, J.R., Arenas, R., Díaz García, F., González Cuadra, P., Gómez-Barreiro, J., Abati, J., Castiñeiras, P., Fernández-Suárez, J., Sánchez Martínez, S., Andonaegui, P., González Clavijo, E., Díez Montes, A., Rubio Pascual, F.J., Valle Aguado, B., 2007. Space and time in the tectonic evolution of the northwestern Iberian Massif: implications for the Variscan belt. In: Hatcher, R.D.Jr., Carlson, M.P., McBride, J.H., Martínez Catalán, J.R. (eds.). 4-D Framework of Continental Crust. Geological Society of America, 200 (Memoirs), 403–423.

Meert, J.G., 2003. A synopsis of events related to the assembly of eastern Gondwana. Tectonophysics, 362, 1–40.

Meinhold, G., Morton, A.C., Fanning, C.M., Frei, D., Howard, J.P., Phillips, R.J., Strogen, D., Whitham, A.G., 2011. Evidence from detrital zircons for recycling of Mesoproterozoic and Neoproterozoic crust recorded in Paleozoic and Mesozoic sandstones of southern Libya. Earth and Planetary Science Letters, 312, 164–175.

Meinhold, G., Morton, A.C., Avigad, D., 2013. New insights into peri-Gondwana paleogeography and the Gondwana super-fan system from detrital zircon U-Pb ages. Gondwana Research, 23, 661–665.

Mezger, J., Gerdes, A., 2016. Early Variscan (Visean) granites in the core of central Pyrenean gneiss domes: implications from laser ablation U-Pb and Th-Pb studies. Gondwana Research, 29, 181–198.

Murphy, J.B., Keppie, J.D., Dostal, J., Nance, R.D., 1999. Neoproterozoic–early Paleozoic evolution of Avalonia. Geological Society of America, 336 (Special Papers), 253–266.

Murphy, J.B., Pisarvesky, S.A., Nance, R.D., Keppie, J.D., 2004. Neoproterozoic–Early Paleozoic evolution of peri-Gondwana terranes: implications for Laurentia-Gondwana connections. International Journal of Earth Sciences, 93, 659–682.

Murphy, J.B., Pisarvesky, S.A., Nance, R.D., 2013. Potential geodynamic relationships between the development of peripheral orogens along the northern margin of Gondwana and the amalgamation of West Gondwana. Mineralogy and Petrology, 107, 635–650.

Nance, D.R., Murphy, J.B., Keppie, J.D., 2002. A Cordilleran model for the evolution of Avalonia. Tectonophysics, 352, 11–31.

Nance, R.D., Murphy, J.B., Strachan, R.B., Keppie, J.D., Gutiérrez-Alonso, G., Fernández-Suárez, J., Quesada, C., Linnemann, U., D'lemos, R., Pisarevsky, S.A., 2008. Neoproterozoic–early Palaeozoic tectonostratigraphy and palaeogeography of the peri-Gondwanan terranes: Amazonian v. West African connections. In: Ennih, N., Liégeois, J.P. (eds.). The Boundaries of the West African Craton. London, The Geological Society, 297 (Special Publication), 345–383.

Padel, M., Clausen, S., Álvaro, J.J., Casas, J.M., 2017a. Review of the Ediacaran–Lower Ordovician (pre–Sardic) stratigraphic framework of the Eastern Pyrenees, southwestern Europe. Geologica Acta, 16(4), 339–355.

Padel, M., Álvaro, J.J., Clausen, S., Guillot, F., Poujol, M., Chichorro, M., Monceret, E., Pereira, M.F., Vizcaïno, D., 2017b. U-Pb laser ablation ICP-MS zircon dating across the Ediacaran–Cambrian transition of the Montagne Noire, southern France. Comptes Rendus Geoscience, 349, 380–390.

Padel, M., Álvaro, J.J., Casas, J.M., Clausen, S., Poujol, M., Sánchez-García, T., 2018. Cadomian volcanosedimentary complexes across the Ediacaran–Cambrian transition of the Eastern Pyrenees, southwestern Europe. International Journal of Earth Sciences, 107, 1579–1601.

Pastor-Galán, D., Gutiérrez-Alonso, G., Fernández-Suárez, J., Murphy, J.B., Nieto, F., 2013. Tectonic evolution of NW Iberia during the Paleozoic inferred from the geochemical record of detrital rocks in the Cantabrian Zone. Lithos, 182–183, 211–228.

Pereira, M.F., Solá, A.R., Chichorro, M., Lope, L., Gerdes, A., Silva, J.B., 2012. North-Gondwana assembly, break-up and paleogeography: U-Pb isotope evidence from detrital and igneous zircons of Ediacaran and Cambrian rocks of SW Iberia. Gondwana Research, 22, 866–881.

Perejón, A., Moreno-Eiris, E., Abad, A., 1994. Montículos de arqueociatos y calcimicrobios del Cámbrico inferior de Terrades, Gerona (Pirineo oriental, España). Boletín de la Real Sociedad Española de Historia Natural (Sección Geológica), 89, 55–95.

Pouclet, A., Álvaro, J.J., Bardintzeff, J.-M., Gil Imaz, A., Monceret, E., Vizcaïno, D., 2017. Cambrian–Early Ordovician volcanism across the South Armorican and Occitan Domains of the Variscan Belt in France: Continental break-up and rifting of the northern Gondwana margin. Geosciences. Frontiers, 8, 25–64.

Shaw, J., Gutiérrez-Alonso, G., Johnston, S.T., Galán, D.P., 2014. Provenance variability along the Early Ordovician north Gondwana margin: paleogeographic and tectonic implications of U-Pb detrital zircon ages from the Armorican Quartzite of the Iberian Variscan belt. Geological Society of America Bulletin, 26, 702–719.

Sláma, J., Košler, J., Condon, D.J., Crowley, J.L., Gerdes, A., Hanchar, J.M., Horstwood, M.S.A., Morris, G.A., Nasdala, L., Norberg, N., Schaltegger, U., Schoene, B., Tubrett, M.N., Whitehouse, M.J., 2008. Plešovice zircon – a new natural reference material for U-Pb and Hf isotopic microanalysis. Chemical Geology, 249, 1–35.

Stampfi, G.M., von Raumer, J., 2008. The birth of the Rheic ocean – Early Paleozoic subsidence patterns and subsequent tectonic plate scenarios. Tectonophysics, 461, 9–20.

Stampfi, G.M., Hochard, C., Vérard, C., Wilhem, C., von Raumer, J., 2013. The formation of Pangea. Tectonophysics, 593, 1-19.

Stern, R.J., 1994. Arc assembly and continental collision in the Neoproterozoic east African orogen: implication for the consolidation of Gondwana. Annual Review of Earth and Planetary Sciences, 22, 319–351.

Talavera, C., Montero, P., Martínez Poyatos, D., Williams, I.S., 2012. Ediacaran to Lower Ordovician age for rocks ascribed to the Schist-Graywacke Complex (Iberian Massif, Spain): evidence from detrital zircon SHRIMP U-Pb geochronology. Gondwana Research, 22, 928–942.

Van Achterbergh, E., Ryan, C.G., Jackson, S.E., Griffin, W.L., 2001. Data reduction software for LA-ICP-MS: appendix. In: Sylvester, P.J. (ed.). Laser Ablation-ICP-mass spectrometry in the Earth Sciences: principles and applications. Mineralogical Association of Canada, Short Courses Series, 29, 239–243.

Vermeesch, P., 2018. IsoplotR: A free and open toolbox for geochronology. Geoscience Frontiers, 9, 1479–1493.

Wallet, E., Padel, M., Devaere, L., Clausen, S., Álvaro, J.J., Laumonier, B., 2022. Cambrian Age 3 small shelly fossils from the Terrades inlier, southern Pyrenees, Spain: biostratigraphic and paleobiogeographic implications. Journal of Paleontology, 96, 552–582.

**Manuscript received December 2021;**
**revision accepted July 2022;**
**published Online October 2022.**

# APPENDIX I

**TABLE I.**

| | | | | Isotopic Ratios | | | | | Apparent Ages | | | | | |
|---|---|---|---|---|---|---|---|---|---|---|---|---|---|---|
| ALN1 | Pb (ppm) | U (ppm) | Th/U | $^{207}Pb/^{235}U$ | 1sigAbsErr | $^{206}Pb/^{238}U$ | 1sigAbsErr | rho | $^{207}Pb/^{206}Pb$ | 1sigAbsErr | $^{206}Pb/^{238}U$ | 1sigAbsErr | $^{207}Pb/^{235}U$ | 1sigAbsErr | Conc.(%) |
| ZR25 | 18 | 164 | 1.9 | 0.628 | 0.008 | 0.078 | 0.001 | 0.85 | 551 | 27 | 483 | 5 | 495 | 5 | 98 |
| ZR15 | 38 | 408 | 1.0 | 0.651 | 0.008 | 0.079 | 0.001 | 0.92 | 586 | 24 | 492 | 5 | 509 | 5 | 97 |
| ZR106 | 108 | 1283 | 0.2 | 0.700 | 0.008 | 0.085 | 0.001 | 0.93 | 583 | 24 | 529 | 6 | 539 | 5 | 98 |
| ZR118 | 245 | 2767 | 0.4 | 0.694 | 0.008 | 0.086 | 0.001 | 0.94 | 555 | 24 | 531 | 6 | 535 | 5 | 99 |
| ZR57 | 54 | 658 | 0.1 | 0.708 | 0.009 | 0.087 | 0.001 | 0.92 | 571 | 24 | 537 | 6 | 544 | 5 | 99 |
| ZR97 | 45 | 480 | 0.6 | 0.730 | 0.009 | 0.088 | 0.001 | 0.92 | 618 | 24 | 542 | 6 | 557 | 5 | 97 |
| ZR99 | 66 | 668 | 0.7 | 0.723 | 0.009 | 0.088 | 0.001 | 0.94 | 593 | 23 | 543 | 6 | 552 | 5 | 98 |
| ZR96 | 18 | 199 | 0.5 | 0.768 | 0.010 | 0.088 | 0.001 | 0.84 | 722 | 27 | 543 | 6 | 579 | 6 | 94 |
| ZR64 | 35 | 412 | 0.1 | 0.733 | 0.009 | 0.089 | 0.001 | 0.90 | 591 | 25 | 551 | 6 | 558 | 5 | 99 |
| ZR7 | 15 | 147 | 0.9 | 0.741 | 0.010 | 0.089 | 0.001 | 0.88 | 612 | 26 | 551 | 6 | 563 | 6 | 98 |
| ZR83 | 188 | 2275 | 0.0 | 0.731 | 0.009 | 0.090 | 0.001 | 0.95 | 575 | 23 | 553 | 6 | 557 | 5 | 99 |
| ZR46 | 54 | 578 | 0.4 | 0.740 | 0.009 | 0.091 | 0.001 | 0.93 | 571 | 24 | 560 | 6 | 562 | 5 | 100 |
| ZR37 | 15 | 173 | 0.2 | 0.736 | 0.009 | 0.091 | 0.001 | 0.91 | 559 | 25 | 561 | 6 | 560 | 5 | 100 |
| ZR50 | 25 | 278 | 0.3 | 0.745 | 0.009 | 0.091 | 0.001 | 0.91 | 582 | 25 | 561 | 6 | 565 | 5 | 99 |
| ZR59 | 30 | 299 | 0.7 | 0.742 | 0.009 | 0.091 | 0.001 | 0.91 | 569 | 25 | 562 | 6 | 564 | 5 | 100 |
| ZR3 | 23 | 258 | 0.2 | 0.777 | 0.009 | 0.092 | 0.001 | 0.94 | 643 | 23 | 568 | 6 | 584 | 5 | 97 |
| ZR117 | 12 | 103 | 1.1 | 0.787 | 0.011 | 0.093 | 0.001 | 0.84 | 657 | 27 | 572 | 6 | 590 | 6 | 97 |
| ZR96 | 63 | 693 | 0.1 | 0.803 | 0.010 | 0.095 | 0.001 | 0.94 | 659 | 23 | 583 | 6 | 599 | 5 | 97 |
| ZR16 | 16 | 165 | 0.4 | 0.772 | 0.010 | 0.095 | 0.001 | 0.89 | 570 | 25 | 584 | 6 | 581 | 6 | 100 |
| ZR12 | 48 | 430 | 0.9 | 0.772 | 0.009 | 0.095 | 0.001 | 0.95 | 562 | 23 | 586 | 6 | 581 | 5 | 101 |
| ZR58 | 67 | 578 | 1.1 | 0.803 | 0.010 | 0.095 | 0.001 | 0.93 | 644 | 24 | 587 | 6 | 598 | 5 | 98 |
| ZR27 | 71 | 779 | 0.1 | 0.812 | 0.010 | 0.095 | 0.001 | 0.94 | 666 | 23 | 587 | 6 | 604 | 5 | 97 |
| ZR104 | 18 | 207 | 0.0 | 0.814 | 0.012 | 0.096 | 0.001 | 0.78 | 665 | 30 | 589 | 6 | 605 | 7 | 97 |
| ZR79 | 70 | 789 | 0.0 | 0.825 | 0.010 | 0.096 | 0.001 | 0.94 | 695 | 23 | 589 | 6 | 611 | 6 | 96 |
| ZR111 | 196 | 2162 | 0.1 | 0.778 | 0.009 | 0.096 | 0.001 | 0.95 | 566 | 23 | 589 | 6 | 584 | 5 | 101 |
| ZR28 | 6 | 56 | 0.9 | 0.779 | 0.012 | 0.096 | 0.001 | 0.72 | 567 | 33 | 590 | 7 | 585 | 7 | 101 |
| ZR4 | 78 | 709 | 0.8 | 0.805 | 0.010 | 0.096 | 0.001 | 0.97 | 634 | 23 | 591 | 6 | 600 | 5 | 99 |
| ZR92 | 23 | 244 | 0.2 | 0.833 | 0.011 | 0.096 | 0.001 | 0.89 | 703 | 25 | 592 | 6 | 615 | 6 | 96 |
| ZR53 | 49 | 539 | 0.1 | 0.791 | 0.010 | 0.096 | 0.001 | 0.93 | 583 | 24 | 594 | 6 | 592 | 5 | 100 |
| ZR103 | 165 | 1762 | 0.2 | 0.802 | 0.009 | 0.097 | 0.001 | 0.96 | 607 | 23 | 595 | 6 | 598 | 5 | 100 |
| ZR38 | 46 | 512 | 0.1 | 0.814 | 0.010 | 0.097 | 0.001 | 0.95 | 637 | 23 | 596 | 6 | 605 | 5 | 99 |
| ZR47 | 14 | 121 | 1.0 | 0.853 | 0.011 | 0.097 | 0.001 | 0.88 | 734 | 25 | 597 | 6 | 626 | 6 | 95 |
| ZR49 | 63 | 654 | 0.2 | 0.859 | 0.011 | 0.098 | 0.001 | 0.87 | 734 | 25 | 601 | 7 | 630 | 6 | 95 |
| ZR115 | 56 | 596 | 0.1 | 0.818 | 0.010 | 0.098 | 0.001 | 0.92 | 627 | 24 | 602 | 6 | 607 | 6 | 99 |
| ZR61 | 30 | 230 | 1.5 | 0.830 | 0.010 | 0.099 | 0.001 | 0.91 | 636 | 24 | 607 | 7 | 613 | 6 | 99 |
| ZR112 | 22 | 220 | 0.3 | 0.847 | 0.011 | 0.099 | 0.001 | 0.89 | 680 | 25 | 608 | 7 | 623 | 6 | 97 |
| ZR19 | 33 | 298 | 0.7 | 0.833 | 0.010 | 0.099 | 0.001 | 0.93 | 637 | 24 | 609 | 7 | 615 | 6 | 99 |
| ZR66 | 57 | 595 | 0.1 | 0.820 | 0.010 | 0.100 | 0.001 | 0.96 | 581 | 23 | 616 | 7 | 608 | 5 | 101 |
| ZR39 | 36 | 355 | 0.3 | 0.848 | 0.010 | 0.101 | 0.001 | 0.94 | 646 | 23 | 617 | 7 | 624 | 6 | 99 |
| ZR95 | 23 | 204 | 0.6 | 0.906 | 0.011 | 0.102 | 0.001 | 0.90 | 751 | 24 | 627 | 7 | 655 | 6 | 96 |
| ZR114 | 33 | 319 | 0.3 | 0.917 | 0.012 | 0.103 | 0.001 | 0.89 | 771 | 25 | 629 | 7 | 661 | 6 | 95 |
| ZR21 | 11 | 104 | 0.4 | 0.862 | 0.012 | 0.103 | 0.001 | 0.84 | 638 | 27 | 630 | 7 | 631 | 6 | 100 |
| ZR69 | 14 | 120 | 0.8 | 0.871 | 0.012 | 0.103 | 0.001 | 0.86 | 658 | 26 | 630 | 7 | 636 | 6 | 99 |
| ZR101 | 33 | 309 | 0.3 | 0.882 | 0.011 | 0.104 | 0.001 | 0.93 | 650 | 23 | 640 | 7 | 642 | 6 | 100 |
| ZR85 | 32 | 292 | 0.6 | 0.914 | 0.012 | 0.104 | 0.001 | 0.88 | 726 | 25 | 640 | 7 | 659 | 6 | 97 |
| ZR52 | 9 | 92 | 0.2 | 0.908 | 0.013 | 0.105 | 0.001 | 0.81 | 699 | 28 | 643 | 7 | 656 | 7 | 98 |
| ZR34 | 13 | 108 | 0.8 | 0.921 | 0.012 | 0.105 | 0.001 | 0.85 | 728 | 26 | 644 | 7 | 663 | 7 | 97 |
| ZR45 | 39 | 372 | 0.3 | 0.902 | 0.012 | 0.106 | 0.001 | 0.87 | 661 | 26 | 650 | 7 | 653 | 6 | 100 |
| ZR26 | 19 | 155 | 0.8 | 0.915 | 0.012 | 0.107 | 0.001 | 0.88 | 682 | 25 | 653 | 7 | 660 | 6 | 99 |
| ZR36 | 46 | 443 | 0.2 | 0.901 | 0.011 | 0.107 | 0.001 | 0.94 | 644 | 23 | 655 | 7 | 652 | 6 | 100 |
| ZR88 | 20 | 172 | 0.6 | 0.944 | 0.012 | 0.107 | 0.001 | 0.88 | 736 | 25 | 657 | 7 | 675 | 6 | 97 |
| ZR113 | 2 | 16 | 0.9 | 0.940 | 0.021 | 0.108 | 0.001 | 0.54 | 717 | 47 | 660 | 8 | 673 | 11 | 98 |
| ZR43 | 29 | 191 | 1.8 | 0.938 | 0.011 | 0.109 | 0.001 | 0.93 | 692 | 24 | 666 | 7 | 672 | 6 | 99 |
| ZR90 | 12 | 102 | 0.6 | 0.947 | 0.013 | 0.109 | 0.001 | 0.80 | 707 | 28 | 667 | 7 | 677 | 7 | 99 |
| ZR80 | 30 | 254 | 0.5 | 0.958 | 0.012 | 0.112 | 0.001 | 0.92 | 678 | 24 | 684 | 7 | 682 | 6 | 100 |
| ZR56 | 21 | 181 | 0.5 | 0.967 | 0.012 | 0.113 | 0.001 | 0.90 | 673 | 25 | 691 | 7 | 687 | 6 | 101 |
| ZR35 | 18 | 138 | 1.0 | 1.003 | 0.013 | 0.114 | 0.001 | 0.90 | 733 | 25 | 697 | 7 | 705 | 6 | 99 |
| ZR75 | 13 | 103 | 0.7 | 1.000 | 0.014 | 0.115 | 0.001 | 0.84 | 715 | 27 | 701 | 8 | 704 | 7 | 100 |
| ZR33 | 20 | 166 | 0.2 | 1.094 | 0.013 | 0.120 | 0.001 | 0.91 | 809 | 23 | 731 | 8 | 750 | 7 | 97 |
| ZR108 | 10 | 78 | 0.7 | 1.057 | 0.015 | 0.120 | 0.001 | 0.81 | 735 | 28 | 732 | 8 | 732 | 7 | 100 |
| ZR89 | 4 | 28 | 0.6 | 1.262 | 0.021 | 0.133 | 0.002 | 0.72 | 894 | 32 | 805 | 9 | 829 | 9 | 97 |
| ZR18 | 32 | 234 | 0.3 | 1.270 | 0.015 | 0.135 | 0.002 | 0.94 | 884 | 23 | 814 | 9 | 833 | 7 | 98 |
| ZR110 | 41 | 280 | 0.5 | 1.276 | 0.016 | 0.137 | 0.002 | 0.92 | 855 | 23 | 828 | 9 | 835 | 7 | 99 |
| ZR62 | 89 | 603 | 0.6 | 1.308 | 0.015 | 0.138 | 0.002 | 0.96 | 890 | 22 | 834 | 9 | 849 | 7 | 98 |
| ZR68 | 44 | 304 | 0.3 | 1.350 | 0.016 | 0.141 | 0.002 | 0.96 | 906 | 22 | 853 | 9 | 868 | 7 | 98 |
| ZR6 | 32 | 216 | 0.4 | 1.378 | 0.017 | 0.144 | 0.002 | 0.94 | 917 | 22 | 865 | 9 | 880 | 7 | 98 |
| ZR54 | 175 | 1030 | 0.9 | 1.441 | 0.017 | 0.145 | 0.002 | 0.94 | 988 | 22 | 873 | 9 | 906 | 7 | 96 |
| ZR84 | 61 | 413 | 0.3 | 1.410 | 0.017 | 0.145 | 0.002 | 0.93 | 944 | 23 | 873 | 9 | 893 | 7 | 98 |
| ZR30 | 47 | 298 | 0.5 | 1.476 | 0.019 | 0.148 | 0.002 | 0.90 | 997 | 23 | 889 | 9 | 921 | 8 | 97 |
| ZR77 | 28 | 180 | 0.4 | 1.450 | 0.018 | 0.152 | 0.002 | 0.93 | 911 | 23 | 910 | 10 | 910 | 7 | 100 |
| ZR22 | 24 | 121 | 1.3 | 1.529 | 0.020 | 0.155 | 0.002 | 0.89 | 972 | 24 | 929 | 10 | 942 | 8 | 99 |
| ZR2 | 22 | 138 | 0.5 | 1.545 | 0.019 | 0.157 | 0.002 | 0.93 | 968 | 22 | 940 | 10 | 948 | 8 | 98 |
| ZR81 | 32 | 192 | 0.6 | 1.546 | 0.019 | 0.159 | 0.002 | 0.90 | 944 | 23 | 951 | 10 | 949 | 8 | 100 |
| ZR78 | 61 | 406 | 0.0 | 1.591 | 0.019 | 0.162 | 0.002 | 0.95 | 965 | 22 | 968 | 10 | 967 | 7 | 100 |
| ZR20 | 68 | 380 | 0.6 | 1.613 | 0.019 | 0.162 | 0.002 | 0.95 | 989 | 22 | 969 | 10 | 975 | 7 | 99 |
| ZR73 | 28 | 204 | 0.5 | 1.271 | 0.015 | 0.127 | 0.001 | 0.92 | 1005 | 22 | 770 | 8 | 833 | 7 | 83 |
| ZR78 | 37 | 201 | 0.6 | 1.707 | 0.021 | 0.170 | 0.002 | 0.94 | 1005 | 22 | 1014 | 11 | 1011 | 8 | 101 |
| ZR72 | 71 | 362 | 0.9 | 1.694 | 0.020 | 0.169 | 0.002 | 0.94 | 1007 | 22 | 1006 | 10 | 1006 | 8 | 100 |

**TABLE I.** Continued

| | | | | Isotopic Ratios | | | | | Apparent Ages | | | | | | |
|---|---|---|---|---|---|---|---|---|---|---|---|---|---|---|---|
| ALN1 | Pb (ppm) | U (ppm) | Th/U | $^{207}Pb/^{235}U$ | 1sigAbsErr | $^{206}Pb/^{238}U$ | 1sigAbsErr | rho | $^{207}Pb/^{206}Pb$ | 1sigAbsErr | $^{206}Pb/^{238}U$ | 1sigAbsErr | $^{207}Pb/^{235}U$ | 1sigAbsErr | Conc.(%) |
| ZR76 | 34 | 209 | 0.2 | 1.642 | 0.020 | 0.164 | 0.002 | 0.93 | 1007 | 22 | 978 | 10 | 987 | 8 | 98 |
| ZR94 | 68 | 382 | 0.7 | 1.589 | 0.019 | 0.158 | 0.002 | 0.94 | 1007 | 22 | 948 | 10 | 966 | 7 | 96 |
| ZR63 | 22 | 112 | 1.1 | 1.631 | 0.020 | 0.162 | 0.002 | 0.90 | 1010 | 23 | 970 | 10 | 982 | 8 | 97 |
| ZR74 | 16 | 63 | 2.2 | 1.698 | 0.023 | 0.169 | 0.002 | 0.85 | 1011 | 25 | 1006 | 11 | 1008 | 9 | 100 |
| ZR70 | 16 | 82 | 0.7 | 1.708 | 0.024 | 0.170 | 0.002 | 0.83 | 1012 | 26 | 1012 | 11 | 1012 | 9 | 100 |
| ZR87 | 31 | 173 | 0.5 | 1.680 | 0.021 | 0.170 | 0.002 | 0.91 | 975 | 23 | 1013 | 11 | 1001 | 8 | 103 |
| ZR23 | 33 | 146 | 1.4 | 1.717 | 0.021 | 0.170 | 0.002 | 0.93 | 1021 | 22 | 1012 | 11 | 1015 | 8 | 99 |
| ZR105 | 36 | 177 | 1.0 | 1.715 | 0.021 | 0.170 | 0.002 | 0.90 | 1021 | 23 | 1011 | 11 | 1014 | 8 | 99 |
| ZR91 | 143 | 879 | 0.4 | 1.590 | 0.018 | 0.157 | 0.002 | 0.98 | 1027 | 21 | 940 | 10 | 966 | 7 | 94 |
| ZR17 | 8 | 41 | 0.9 | 1.667 | 0.023 | 0.164 | 0.002 | 0.84 | 1029 | 25 | 981 | 10 | 996 | 9 | 97 |
| ZR71 | 53 | 255 | 1.2 | 1.677 | 0.021 | 0.165 | 0.002 | 0.92 | 1030 | 23 | 986 | 10 | 1000 | 8 | 97 |
| ZR32 | 30 | 156 | 1.0 | 1.648 | 0.020 | 0.162 | 0.002 | 0.93 | 1040 | 22 | 966 | 10 | 989 | 8 | 95 |
| ZR40 | 14 | 75 | 0.7 | 1.733 | 0.022 | 0.170 | 0.002 | 0.89 | 1040 | 24 | 1012 | 11 | 1021 | 8 | 98 |
| ZR41 | 21 | 117 | 0.5 | 1.791 | 0.022 | 0.174 | 0.002 | 0.93 | 1058 | 23 | 1035 | 11 | 1042 | 8 | 99 |
| ZR5 | 47 | 255 | 0.9 | 1.652 | 0.020 | 0.161 | 0.002 | 0.94 | 1059 | 22 | 960 | 10 | 990 | 8 | 94 |
| ZR1 | 20 | 98 | 1.0 | 1.803 | 0.022 | 0.175 | 0.002 | 0.94 | 1063 | 22 | 1039 | 11 | 1047 | 8 | 98 |
| ZR65 | 122 | 778 | 0.5 | 1.513 | 0.018 | 0.146 | 0.002 | 0.96 | 1076 | 21 | 877 | 9 | 936 | 7 | 87 |
| ZR98 | 109 | 592 | 0.2 | 2.002 | 0.023 | 0.186 | 0.002 | 0.97 | 1145 | 21 | 1102 | 11 | 1116 | 8 | 97 |
| ZR100 | 8 | 77 | 0.2 | 1.113 | 0.018 | 0.096 | 0.001 | 0.72 | 1300 | 30 | 590 | 7 | 760 | 9 | 58 |
| ZR60 | 12 | 41 | 1.2 | 2.835 | 0.037 | 0.233 | 0.003 | 0.87 | 1389 | 23 | 1350 | 14 | 1365 | 10 | 98 |
| ZR67 | 201 | 823 | 0.5 | 3.177 | 0.037 | 0.217 | 0.002 | 0.98 | 1735 | 19 | 1266 | 13 | 1452 | 9 | 84 |
| ZR9 | 54 | 142 | 1.1 | 4.593 | 0.054 | 0.310 | 0.004 | 0.96 | 1758 | 19 | 1740 | 17 | 1748 | 10 | 99 |
| ZR107 | 62 | 230 | 0.2 | 3.918 | 0.046 | 0.264 | 0.003 | 0.96 | 1759 | 19 | 1511 | 15 | 1617 | 9 | 92 |
| ZR93 | 105 | 367 | 0.2 | 4.253 | 0.049 | 0.281 | 0.003 | 0.97 | 1797 | 19 | 1595 | 16 | 1684 | 10 | 94 |
| ZR14 | 16 | 48 | 0.6 | 4.820 | 0.061 | 0.304 | 0.004 | 0.91 | 1878 | 21 | 1713 | 17 | 1788 | 11 | 95 |
| ZR109 | 59 | 198 | 0.1 | 4.841 | 0.057 | 0.299 | 0.003 | 0.95 | 1918 | 19 | 1686 | 17 | 1792 | 10 | 93 |
| ZR42 | 117 | 324 | 0.6 | 5.318 | 0.062 | 0.323 | 0.004 | 0.97 | 1946 | 19 | 1806 | 18 | 1872 | 10 | 96 |
| ZR82 | 116 | 360 | 0.8 | 4.571 | 0.055 | 0.276 | 0.003 | 0.94 | 1955 | 19 | 1574 | 16 | 1744 | 10 | 89 |
| ZR10 | 111 | 283 | 1.0 | 5.397 | 0.063 | 0.324 | 0.004 | 0.98 | 1966 | 18 | 1811 | 18 | 1884 | 10 | 96 |
| ZR11 | 39 | 85 | 1.6 | 5.659 | 0.069 | 0.338 | 0.004 | 0.94 | 1976 | 20 | 1879 | 19 | 1925 | 11 | 97 |
| ZR13 | 21 | 51 | 0.6 | 6.206 | 0.074 | 0.365 | 0.004 | 0.95 | 2005 | 19 | 2006 | 20 | 2005 | 10 | 100 |
| ZR24 | 36 | 103 | 0.5 | 5.381 | 0.065 | 0.316 | 0.004 | 0.94 | 2007 | 19 | 1771 | 18 | 1882 | 10 | 94 |
| ZR102 | 208 | 582 | 0.4 | 5.783 | 0.067 | 0.328 | 0.004 | 0.97 | 2067 | 18 | 1831 | 18 | 1944 | 10 | 94 |
| ZR51 | 186 | 441 | 0.6 | 6.691 | 0.079 | 0.374 | 0.004 | 0.96 | 2093 | 19 | 2050 | 20 | 2071 | 10 | 99 |
| ZR116 | 56 | 141 | 0.5 | 6.462 | 0.078 | 0.359 | 0.004 | 0.93 | 2105 | 19 | 1978 | 19 | 2041 | 11 | 97 |
| ZR48 | 183 | 458 | 0.4 | 6.776 | 0.079 | 0.371 | 0.004 | 0.96 | 2131 | 18 | 2034 | 20 | 2083 | 10 | 98 |
| ZR31 | 69 | 109 | 1.3 | 11.235 | 0.130 | 0.469 | 0.005 | 0.97 | 2594 | 17 | 2480 | 23 | 2543 | 11 | 98 |
| ZR44 | 534 | 1190 | 0.1 | 10.341 | 0.119 | 0.429 | 0.005 | 0.97 | 2604 | 17 | 2302 | 22 | 2466 | 11 | 95 |
| ZR86 | 132 | 284 | 0.6 | 9.642 | 0.115 | 0.396 | 0.004 | 0.94 | 2621 | 18 | 2150 | 21 | 2401 | 11 | 92 |
| ZR55 | 109 | 206 | 0.4 | 11.496 | 0.136 | 0.472 | 0.005 | 0.95 | 2623 | 18 | 2491 | 23 | 2564 | 11 | 98 |
| ZR8 | 93 | 154 | 0.7 | 12.907 | 0.150 | 0.503 | 0.006 | 0.98 | 2708 | 17 | 2627 | 25 | 2673 | 11 | 99 |
| ZR29 | 212 | 277 | 0.5 | 23.846 | 0.285 | 0.278 | 0.003 | 0.95 | 4562 | 16 | 1580 | 16 | 3262 | 12 | 72 |

**TABLE II.**

| | | | | Isotopic Ratios | | | | | Apparent Ages | | | | | | |
|---|---|---|---|---|---|---|---|---|---|---|---|---|---|---|---|
| mpad8 | Pb (ppm) | U (ppm) | Th/U | $^{207}Pb/^{235}U$ | 1sigAbsErr | $^{206}Pb/^{238}U$ | 1sigAbsErr | rho | $^{207}Pb/^{206}Pb$ | 1sigAbsErr | $^{206}Pb/^{238}U$ | 1sigAbsErr | $^{207}Pb/^{235}U$ | 1sigAbsErr | Conc.(%) |
| ZR101 | 101 | 1035 | 0.9 | 0.666 | 0.008 | 0.0820 | 0.0009 | 0.91 | 565 | 25 | 508 | 5 | 518 | 5 | 98 |
| ZR111 | 24 | 268 | 0.6 | 0.726 | 0.009 | 0.0834 | 0.0009 | 0.86 | 712 | 26 | 516 | 6 | 554 | 6 | 93 |
| ZR46 | 36 | 386 | 0.6 | 0.708 | 0.009 | 0.0852 | 0.0009 | 0.87 | 612 | 26 | 527 | 6 | 543 | 5 | 97 |
| ZR42 | 21 | 267 | 0.0 | 0.711 | 0.009 | 0.0856 | 0.0010 | 0.85 | 613 | 27 | 530 | 6 | 545 | 6 | 97 |
| ZR36 | 84 | 874 | 0.7 | 0.754 | 0.009 | 0.0876 | 0.0010 | 0.94 | 690 | 23 | 541 | 6 | 571 | 5 | 95 |
| ZR48 | 92 | 912 | 0.7 | 0.743 | 0.009 | 0.0901 | 0.0010 | 0.93 | 598 | 24 | 556 | 6 | 564 | 5 | 99 |
| ZR4 | 23 | 191 | 1.3 | 0.764 | 0.011 | 0.0907 | 0.0010 | 0.81 | 642 | 28 | 560 | 6 | 576 | 6 | 97 |
| ZR107 | 35 | 360 | 0.5 | 0.759 | 0.009 | 0.0920 | 0.0010 | 0.88 | 598 | 25 | 567 | 6 | 574 | 5 | 99 |
| ZR108 | 29 | 327 | 0.2 | 0.752 | 0.009 | 0.0928 | 0.0010 | 0.88 | 560 | 26 | 572 | 6 | 569 | 6 | 100 |
| ZR52 | 38 | 294 | 1.6 | 0.749 | 0.009 | 0.0928 | 0.0010 | 0.87 | 550 | 26 | 572 | 6 | 568 | 6 | 101 |
| ZR7 | 23 | 199 | 1.1 | 0.782 | 0.011 | 0.0931 | 0.0011 | 0.82 | 639 | 28 | 574 | 6 | 587 | 6 | 98 |
| ZR78 | 95 | 780 | 1.4 | 0.788 | 0.009 | 0.0942 | 0.0010 | 0.92 | 629 | 24 | 580 | 6 | 590 | 5 | 98 |
| ZR28 | 158 | 1769 | 0.1 | 0.825 | 0.01 | 0.0946 | 0.0011 | 0.90 | 717 | 24 | 583 | 6 | 611 | 6 | 95 |
| ZR47 | 39 | 355 | 0.7 | 0.809 | 0.01 | 0.0950 | 0.0011 | 0.91 | 667 | 24 | 585 | 6 | 602 | 6 | 97 |
| ZR37 | 25 | 272 | 0.1 | 0.796 | 0.01 | 0.0958 | 0.0011 | 0.92 | 612 | 24 | 590 | 6 | 595 | 6 | 99 |
| ZR95 | 122 | 1362 | 0.0 | 0.827 | 0.01 | 0.0963 | 0.0011 | 0.94 | 685 | 23 | 593 | 6 | 612 | 5 | 97 |
| ZR24 | 29 | 216 | 1.3 | 0.888 | 0.012 | 0.0964 | 0.0011 | 0.84 | 832 | 26 | 593 | 6 | 645 | 7 | 92 |
| ZR72 | 97 | 971 | 0.4 | 0.817 | 0.009 | 0.0968 | 0.0011 | 0.94 | 647 | 23 | 596 | 6 | 606 | 5 | 98 |
| ZR54 | 26 | 214 | 1.0 | 0.815 | 0.011 | 0.0970 | 0.0011 | 0.85 | 639 | 27 | 597 | 6 | 605 | 6 | 99 |
| ZR20 | 13 | 124 | 0.5 | 0.809 | 0.011 | 0.0975 | 0.0011 | 0.82 | 611 | 28 | 600 | 7 | 602 | 6 | 100 |
| ZR25 | 22 | 199 | 0.7 | 0.955 | 0.013 | 0.0977 | 0.0011 | 0.84 | 956 | 26 | 601 | 7 | 681 | 7 | 88 |
| ZR76 | 154 | 1400 | 0.7 | 0.83 | 0.01 | 0.0978 | 0.0011 | 0.93 | 660 | 23 | 601 | 6 | 614 | 5 | 98 |
| ZR32 | 11 | 83 | 1.6 | 0.812 | 0.012 | 0.0979 | 0.0011 | 0.78 | 609 | 30 | 602 | 7 | 603 | 7 | 100 |
| ZR45 | 19 | 161 | 0.9 | 0.817 | 0.011 | 0.0979 | 0.0011 | 0.85 | 622 | 26 | 602 | 6 | 607 | 6 | 99 |
| ZR57 | 83 | 755 | 0.6 | 0.85 | 0.01 | 0.0980 | 0.0011 | 0.90 | 707 | 24 | 602 | 6 | 625 | 6 | 96 |
| ZR59 | 29 | 267 | 0.6 | 0.845 | 0.011 | 0.0985 | 0.0011 | 0.83 | 681 | 27 | 606 | 6 | 622 | 6 | 97 |
| ZR43 | 33 | 315 | 0.5 | 0.824 | 0.01 | 0.0985 | 0.0011 | 0.90 | 626 | 25 | 606 | 6 | 610 | 6 | 99 |
| ZR12 | 19 | 180 | 0.5 | 0.879 | 0.012 | 0.0985 | 0.0011 | 0.81 | 766 | 28 | 606 | 7 | 641 | 7 | 95 |
| ZR31 | 22 | 170 | 0.9 | 0.81 | 0.011 | 0.0986 | 0.0011 | 0.85 | 589 | 27 | 606 | 7 | 603 | 6 | 101 |
| ZR2 | 24 | 214 | 0.7 | 0.822 | 0.01 | 0.0987 | 0.0011 | 0.89 | 618 | 25 | 607 | 7 | 609 | 6 | 100 |
| ZR16 | 55 | 542 | 0.3 | 0.847 | 0.011 | 0.0992 | 0.0011 | 0.89 | 673 | 25 | 609 | 7 | 623 | 6 | 98 |
| ZR92 | 17 | 158 | 0.4 | 0.825 | 0.011 | 0.0996 | 0.0011 | 0.84 | 607 | 27 | 612 | 6 | 611 | 6 | 100 |
| ZR3 | 18 | 146 | 1.2 | 0.857 | 0.011 | 0.1004 | 0.0011 | 0.87 | 670 | 26 | 617 | 7 | 628 | 6 | 98 |
| ZR14 | 17 | 129 | 1.3 | 0.844 | 0.011 | 0.1006 | 0.0011 | 0.85 | 636 | 27 | 618 | 7 | 622 | 6 | 99 |
| ZR8 | 99 | 979 | 0.3 | 0.882 | 0.011 | 0.1009 | 0.0011 | 0.94 | 722 | 23 | 620 | 7 | 642 | 6 | 97 |
| ZR40 | 11 | 79 | 1.3 | 0.869 | 0.014 | 0.1011 | 0.0012 | 0.69 | 687 | 34 | 621 | 7 | 635 | 8 | 98 |
| ZR33 | 33 | 318 | 0.3 | 0.864 | 0.011 | 0.1025 | 0.0012 | 0.90 | 645 | 25 | 629 | 7 | 633 | 6 | 100 |
| ZR68 | 118 | 1214 | 0.1 | 0.88 | 0.01 | 0.1033 | 0.0011 | 0.95 | 669 | 23 | 633 | 7 | 641 | 5 | 99 |
| ZR79 | 31 | 264 | 0.7 | 0.87 | 0.011 | 0.1035 | 0.0011 | 0.87 | 639 | 26 | 635 | 7 | 636 | 6 | 100 |
| ZR22 | 17 | 168 | 0.2 | 0.889 | 0.012 | 0.1039 | 0.0012 | 0.84 | 676 | 27 | 637 | 7 | 646 | 6 | 99 |
| ZR64 | 13 | 121 | 0.4 | 0.894 | 0.012 | 0.1043 | 0.0011 | 0.84 | 681 | 27 | 639 | 7 | 649 | 6 | 99 |
| ZR58 | 5 | 39 | 1.4 | 0.873 | 0.015 | 0.1043 | 0.0012 | 0.65 | 628 | 37 | 640 | 7 | 637 | 8 | 100 |
| ZR50 | 39 | 377 | 0.1 | 0.933 | 0.012 | 0.1051 | 0.0012 | 0.89 | 755 | 24 | 644 | 7 | 669 | 6 | 96 |
| ZR66 | 35 | 305 | 0.6 | 0.901 | 0.011 | 0.1058 | 0.0011 | 0.90 | 666 | 24 | 648 | 7 | 652 | 6 | 99 |
| ZR35 | 32 | 237 | 1.2 | 0.894 | 0.011 | 0.1063 | 0.0012 | 0.89 | 638 | 25 | 651 | 7 | 648 | 6 | 100 |
| ZR83 | 40 | 368 | 0.3 | 0.924 | 0.011 | 0.1085 | 0.0012 | 0.88 | 667 | 25 | 664 | 7 | 665 | 6 | 100 |
| ZR94 | 79 | 692 | 0.4 | 0.942 | 0.011 | 0.1093 | 0.0012 | 0.94 | 692 | 23 | 669 | 7 | 674 | 6 | 99 |
| ZR84 | 27 | 217 | 0.7 | 0.95 | 0.012 | 0.1094 | 0.0012 | 0.85 | 708 | 26 | 669 | 7 | 678 | 6 | 99 |
| ZR69 | 23 | 191 | 0.5 | 0.947 | 0.012 | 0.1097 | 0.0012 | 0.88 | 695 | 25 | 671 | 7 | 676 | 6 | 99 |
| ZR23 | 45 | 419 | 0.1 | 0.973 | 0.012 | 0.1123 | 0.0013 | 0.90 | 703 | 25 | 686 | 7 | 690 | 6 | 99 |
| ZR96 | 28 | 240 | 0.3 | 0.981 | 0.012 | 0.1143 | 0.0013 | 0.91 | 683 | 24 | 697 | 7 | 694 | 6 | 101 |
| ZR29 | 9 | 68 | 0.6 | 1.088 | 0.023 | 0.1188 | 0.0014 | 0.57 | 821 | 43 | 723 | 8 | 748 | 11 | 97 |
| ZR26 | 6 | 37 | 1.0 | 1.149 | 0.019 | 0.1232 | 0.0014 | 0.71 | 858 | 33 | 749 | 8 | 777 | 9 | 96 |
| ZR10 | 12 | 101 | 0.2 | 1.14 | 0.015 | 0.1256 | 0.0014 | 0.85 | 802 | 26 | 763 | 8 | 773 | 7 | 99 |
| ZR81 | 7 | 50 | 0.4 | 1.135 | 0.018 | 0.1263 | 0.0014 | 0.72 | 781 | 32 | 767 | 8 | 770 | 8 | 100 |
| ZR39 | 99 | 756 | 0.3 | 1.225 | 0.014 | 0.1289 | 0.0014 | 0.94 | 898 | 22 | 781 | 8 | 812 | 7 | 96 |
| ZR44 | 46 | 332 | 0.4 | 1.233 | 0.015 | 0.1328 | 0.0015 | 0.92 | 848 | 23 | 804 | 8 | 816 | 7 | 99 |
| ZR11 | 9 | 58 | 0.5 | 1.246 | 0.018 | 0.1349 | 0.0015 | 0.78 | 838 | 29 | 816 | 9 | 821 | 8 | 99 |
| ZR60 | 9 | 60 | 0.5 | 1.253 | 0.018 | 0.1353 | 0.0015 | 0.77 | 843 | 29 | 818 | 9 | 825 | 8 | 99 |
| ZR27 | 22 | 143 | 0.7 | 1.244 | 0.016 | 0.1357 | 0.0015 | 0.86 | 822 | 26 | 820 | 9 | 821 | 7 | 100 |
| ZR85 | 92 | 666 | 0.3 | 1.264 | 0.015 | 0.1366 | 0.0015 | 0.90 | 841 | 24 | 826 | 8 | 830 | 7 | 100 |
| ZR21 | 50 | 338 | 0.3 | 1.381 | 0.017 | 0.1443 | 0.0016 | 0.92 | 911 | 23 | 869 | 9 | 881 | 7 | 99 |
| ZR34 | 34 | 186 | 0.9 | 1.498 | 0.018 | 0.1548 | 0.0017 | 0.93 | 934 | 23 | 928 | 10 | 930 | 7 | 100 |
| ZR103 | 56 | 320 | 0.6 | 1.534 | 0.018 | 0.1562 | 0.0017 | 0.92 | 965 | 23 | 935 | 10 | 944 | 7 | 99 |
| ZR41 | 60 | 345 | 0.5 | 1.594 | 0.019 | 0.1605 | 0.0018 | 0.93 | 988 | 22 | 959 | 10 | 968 | 8 | 99 |
| ZR89 | 270 | 1660 | 0.7 | 1.434 | 0.017 | 0.1433 | 0.0016 | 0.90 | 1003 | 23 | 863 | 9 | 903 | 7 | 90 |
| ZR102 | 46 | 307 | 0.4 | 1.402 | 0.017 | 0.1399 | 0.0015 | 0.89 | 1005 | 23 | 844 | 9 | 890 | 7 | 89 |
| ZR38 | 55 | 297 | 1.0 | 1.562 | 0.019 | 0.1555 | 0.0017 | 0.93 | 1009 | 22 | 932 | 10 | 955 | 7 | 95 |
| ZR30 | 56 | 337 | 0.2 | 1.664 | 0.021 | 0.1656 | 0.0019 | 0.90 | 1011 | 23 | 988 | 10 | 995 | 8 | 98 |
| ZR18 | 27 | 153 | 0.7 | 1.581 | 0.02 | 0.1569 | 0.0018 | 0.88 | 1017 | 24 | 939 | 10 | 963 | 8 | 95 |
| ZR73 | 23 | 126 | 0.8 | 1.618 | 0.021 | 0.1599 | 0.0018 | 0.86 | 1026 | 25 | 956 | 10 | 977 | 8 | 95 |
| ZR70 | 31 | 139 | 1.2 | 1.766 | 0.021 | 0.1737 | 0.0019 | 0.90 | 1035 | 23 | 1032 | 10 | 1033 | 8 | 100 |
| ZR106 | 32 | 147 | 1.2 | 1.698 | 0.021 | 0.1669 | 0.0018 | 0.90 | 1037 | 23 | 995 | 10 | 1008 | 8 | 97 |
| ZR61 | 26 | 150 | 0.9 | 1.479 | 0.021 | 0.1453 | 0.0016 | 0.78 | 1037 | 28 | 874 | 9 | 922 | 9 | 89 |

**TABLE II.** Continued

| | | | | Isotopic Ratios | | | | | Apparent Ages | | | | | | |
|---|---|---|---|---|---|---|---|---|---|---|---|---|---|---|---|
| mpad8 | Pb (ppm) | U (ppm) | Th/U | $^{207}Pb/^{235}U$ | 1sigAbsErr | $^{206}Pb/^{238}U$ | 1sigAbsErr | rho | $^{207}Pb/^{206}Pb$ | 1sigAbsErr | $^{206}Pb/^{238}U$ | 1sigAbsErr | $^{207}Pb/^{235}U$ | 1sigAbsErr | Conc.(%) |
| ZR90 | 80 | 429 | 0.4 | 1.812 | 0.022 | 0.1772 | 0.0019 | 0.89 | 1047 | 23 | 1051 | 11 | 1050 | 8 | 100 |
| ZR75 | 46 | 212 | 1.1 | 1.786 | 0.021 | 0.1741 | 0.0019 | 0.91 | 1052 | 23 | 1035 | 10 | 1040 | 8 | 99 |
| ZR80 | 11 | 93 | 0.9 | 1.019 | 0.015 | 0.0994 | 0.0011 | 0.74 | 1052 | 30 | 611 | 7 | 713 | 8 | 68 |
| ZR93 | 26 | 128 | 0.6 | 1.99 | 0.025 | 0.1782 | 0.0020 | 0.88 | 1222 | 23 | 1057 | 11 | 1112 | 8 | 91 |
| ZR6 | 43 | 211 | 0.2 | 2.367 | 0.029 | 0.2075 | 0.0023 | 0.92 | 1263 | 22 | 1216 | 13 | 1233 | 9 | 98 |
| ZR65 | 283 | 742 | 1.0 | 4.608 | 0.052 | 0.3068 | 0.0033 | 0.96 | 1782 | 19 | 1725 | 16 | 1751 | 9 | 99 |
| ZR109 | 68 | 178 | 0.9 | 4.973 | 0.059 | 0.3155 | 0.0035 | 0.93 | 1870 | 20 | 1768 | 17 | 1815 | 10 | 97 |
| ZR100 | 17 | 36 | 1.5 | 5.354 | 0.066 | 0.3376 | 0.0037 | 0.90 | 1881 | 21 | 1875 | 18 | 1878 | 11 | 100 |
| ZR55 | 443 | 1571 | 0.5 | 4.095 | 0.048 | 0.2561 | 0.0028 | 0.93 | 1895 | 20 | 1470 | 14 | 1653 | 10 | 87 |
| ZR104 | 354 | 841 | 1.0 | 5.641 | 0.065 | 0.3405 | 0.0037 | 0.95 | 1959 | 19 | 1889 | 18 | 1922 | 10 | 98 |
| ZR74 | 86 | 238 | 0.5 | 5.424 | 0.063 | 0.3241 | 0.0035 | 0.93 | 1977 | 20 | 1810 | 17 | 1889 | 10 | 96 |
| ZR71 | 107 | 237 | 1.0 | 6.151 | 0.07 | 0.3640 | 0.0039 | 0.94 | 1994 | 19 | 2001 | 19 | 1998 | 10 | 100 |
| ZR5 | 139 | 422 | 0.1 | 5.57 | 0.065 | 0.3270 | 0.0037 | 0.96 | 2008 | 19 | 1824 | 18 | 1911 | 10 | 95 |
| ZR62 | 82 | 208 | 0.4 | 6.317 | 0.071 | 0.3653 | 0.0039 | 0.96 | 2035 | 19 | 2007 | 19 | 2021 | 10 | 99 |
| ZR19 | 54 | 126 | 0.8 | 6.211 | 0.074 | 0.3546 | 0.0040 | 0.94 | 2058 | 19 | 1957 | 19 | 2006 | 10 | 98 |
| ZR15 | 127 | 300 | 0.5 | 6.879 | 0.081 | 0.3829 | 0.0043 | 0.96 | 2102 | 19 | 2090 | 20 | 2096 | 10 | 100 |
| ZR98 | 320 | 879 | 0.2 | 6.516 | 0.074 | 0.3500 | 0.0038 | 0.96 | 2165 | 18 | 1935 | 18 | 2048 | 10 | 95 |
| ZR88 | 60 | 132 | 0.5 | 7.563 | 0.092 | 0.4030 | 0.0044 | 0.90 | 2178 | 20 | 2183 | 20 | 2181 | 11 | 100 |
| ZR110 | 71 | 164 | 0.3 | 7.617 | 0.09 | 0.4007 | 0.0044 | 0.93 | 2201 | 19 | 2172 | 20 | 2187 | 11 | 99 |
| ZR99 | 45 | 109 | 0.4 | 8.437 | 0.1 | 0.3673 | 0.0041 | 0.93 | 2524 | 19 | 2017 | 19 | 2279 | 11 | 90 |
| ZR112 | 40 | 104 | 0.6 | 7.426 | 0.092 | 0.3221 | 0.0036 | 0.90 | 2530 | 20 | 1800 | 18 | 2164 | 11 | 86 |
| ZR9 | 118 | 211 | 1.1 | 10.022 | 0.117 | 0.4265 | 0.0048 | 0.96 | 2562 | 18 | 2290 | 22 | 2437 | 11 | 95 |
| ZR63 | 435 | 1038 | 0.0 | 9.744 | 0.108 | 0.4121 | 0.0044 | 0.97 | 2573 | 17 | 2224 | 20 | 2411 | 10 | 94 |
| ZR51 | 246 | 442 | 0.6 | 11.308 | 0.131 | 0.4756 | 0.0052 | 0.95 | 2582 | 18 | 2508 | 23 | 2549 | 11 | 99 |
| ZR77 | 207 | 394 | 0.5 | 10.985 | 0.126 | 0.4597 | 0.0050 | 0.94 | 2590 | 18 | 2438 | 22 | 2522 | 11 | 97 |
| ZR105 | 471 | 980 | 0.6 | 9.759 | 0.112 | 0.4060 | 0.0045 | 0.95 | 2600 | 18 | 2197 | 20 | 2412 | 11 | 93 |
| ZR53 | 70 | 121 | 0.8 | 11.22 | 0.133 | 0.4628 | 0.0051 | 0.93 | 2614 | 18 | 2452 | 22 | 2542 | 11 | 97 |
| ZR82 | 141 | 250 | 0.7 | 11.321 | 0.133 | 0.4648 | 0.0050 | 0.92 | 2622 | 18 | 2461 | 22 | 2550 | 11 | 97 |
| ZR56 | 301 | 719 | 0.1 | 9.67 | 0.114 | 0.3963 | 0.0043 | 0.93 | 2625 | 18 | 2152 | 20 | 2404 | 11 | 92 |
| ZR86 | 45 | 79 | 0.7 | 12.084 | 0.146 | 0.4811 | 0.0053 | 0.90 | 2673 | 19 | 2532 | 23 | 2611 | 11 | 98 |
| ZR97 | 226 | 396 | 1.1 | 10.95 | 0.124 | 0.4349 | 0.0048 | 0.96 | 2677 | 17 | 2328 | 21 | 2519 | 11 | 94 |
| ZR91 | 107 | 184 | 0.7 | 12.45 | 0.141 | 0.4739 | 0.0052 | 0.97 | 2747 | 17 | 2501 | 23 | 2639 | 11 | 95 |
| ZR49 | 89 | 172 | 0.1 | 13.302 | 0.155 | 0.4819 | 0.0053 | 0.95 | 2828 | 18 | 2536 | 23 | 2701 | 11 | 96 |

**TABLE III.**

| | | | | Isotopic Ratios | | | | | Apparent Ages | | | | | | |
|---|---|---|---|---|---|---|---|---|---|---|---|---|---|---|---|
| PC7 | Pb (ppm) | U (ppm) | Th/U | 207Pb/235U | 1sigAbsErr | 206Pb/238U | 1sigAbsErr | rho | 207Pb/206Pb | 1sigAbsErr | 206Pb/238U | 1sigAbsErr | 207Pb/235U | 1sigAbsErr | Conc.(%) |
| ZR16 | 19 | 206 | 0.7 | 0.704 | 0.009 | 0.0851 | 0.0010 | 0.90 | 604 | 25 | 527 | 6 | 541 | 5 | 97 |
| ZR20 | 39 | 444 | 0.4 | 0.708 | 0.010 | 0.0853 | 0.0010 | 0.84 | 611 | 27 | 528 | 6 | 544 | 6 | 97 |
| ZR23 | 94 | 922 | 0.9 | 0.714 | 0.009 | 0.0869 | 0.0010 | 0.94 | 591 | 24 | 537 | 6 | 547 | 5 | 98 |
| ZR56 | 19 | 209 | 0.2 | 0.821 | 0.012 | 0.0938 | 0.0011 | 0.77 | 724 | 30 | 578 | 6 | 608 | 7 | 95 |
| ZR3 | 17 | 176 | 0.4 | 0.796 | 0.010 | 0.0942 | 0.0011 | 0.90 | 650 | 25 | 580 | 6 | 595 | 6 | 98 |
| ZR54 | 34 | 352 | 0.3 | 0.792 | 0.010 | 0.0954 | 0.0011 | 0.93 | 612 | 24 | 588 | 6 | 593 | 6 | 99 |
| ZR41 | 12 | 107 | 0.8 | 0.797 | 0.012 | 0.0956 | 0.0011 | 0.77 | 621 | 31 | 589 | 7 | 595 | 7 | 99 |
| ZR74 | 58 | 591 | 0.4 | 0.821 | 0.010 | 0.0966 | 0.0011 | 0.92 | 662 | 24 | 595 | 7 | 609 | 6 | 98 |
| ZR107 | 34 | 277 | 1.2 | 0.826 | 0.010 | 0.0971 | 0.0011 | 0.94 | 664 | 23 | 597 | 7 | 611 | 6 | 98 |
| ZR77 | 35 | 365 | 0.3 | 0.806 | 0.010 | 0.0973 | 0.0011 | 0.95 | 608 | 23 | 599 | 7 | 600 | 6 | 100 |
| ZR32 | 8 | 67 | 1.0 | 0.809 | 0.012 | 0.0974 | 0.0011 | 0.75 | 614 | 32 | 599 | 7 | 602 | 7 | 100 |
| ZR52 | 17 | 174 | 0.2 | 0.826 | 0.012 | 0.0975 | 0.0011 | 0.83 | 656 | 28 | 600 | 7 | 611 | 6 | 98 |
| ZR18 | 32 | 319 | 0.4 | 0.811 | 0.010 | 0.0977 | 0.0011 | 0.95 | 610 | 23 | 601 | 7 | 603 | 5 | 100 |
| ZR27 | 24 | 215 | 0.8 | 0.811 | 0.010 | 0.0977 | 0.0011 | 0.92 | 610 | 24 | 601 | 7 | 603 | 6 | 100 |
| ZR35 | 23 | 226 | 0.4 | 0.813 | 0.010 | 0.0978 | 0.0011 | 0.93 | 615 | 24 | 601 | 7 | 604 | 6 | 100 |
| ZR61 | 12 | 109 | 0.8 | 0.816 | 0.011 | 0.0978 | 0.0011 | 0.84 | 623 | 27 | 602 | 7 | 606 | 6 | 99 |
| ZR8 | 21 | 216 | 0.3 | 0.828 | 0.012 | 0.0979 | 0.0011 | 0.82 | 652 | 28 | 602 | 7 | 613 | 6 | 98 |
| ZR12 | 50 | 547 | 0.0 | 0.841 | 0.011 | 0.0986 | 0.0011 | 0.86 | 671 | 26 | 606 | 7 | 620 | 6 | 98 |
| ZR38 | 13 | 121 | 0.6 | 0.808 | 0.010 | 0.0988 | 0.0011 | 0.88 | 580 | 26 | 607 | 7 | 602 | 6 | 101 |
| ZR72 | 10 | 94 | 0.4 | 0.836 | 0.011 | 0.0991 | 0.0011 | 0.84 | 647 | 27 | 609 | 7 | 617 | 6 | 99 |
| ZR101 | 17 | 167 | 0.4 | 0.826 | 0.011 | 0.0991 | 0.0011 | 0.88 | 619 | 26 | 609 | 7 | 611 | 6 | 100 |
| ZR110 | 20 | 189 | 0.6 | 0.853 | 0.011 | 0.0992 | 0.0011 | 0.90 | 688 | 25 | 610 | 7 | 627 | 6 | 97 |
| ZR51 | 36 | 375 | 0.1 | 0.841 | 0.010 | 0.0995 | 0.0011 | 0.95 | 651 | 23 | 611 | 7 | 620 | 6 | 99 |
| ZR113 | 8 | 56 | 1.6 | 0.837 | 0.012 | 0.0998 | 0.0012 | 0.81 | 632 | 29 | 613 | 7 | 617 | 7 | 99 |
| ZR5 | 10 | 97 | 0.2 | 0.837 | 0.011 | 0.1005 | 0.0011 | 0.85 | 617 | 27 | 617 | 7 | 617 | 6 | 100 |
| ZR13 | 14 | 118 | 1.0 | 0.843 | 0.011 | 0.1007 | 0.0011 | 0.85 | 630 | 27 | 619 | 7 | 621 | 6 | 100 |
| ZR1 | 5 | 40 | 0.7 | 0.833 | 0.013 | 0.1014 | 0.0012 | 0.74 | 587 | 32 | 623 | 7 | 615 | 7 | 101 |
| ZR68 | 9 | 79 | 0.8 | 0.868 | 0.012 | 0.1021 | 0.0012 | 0.84 | 663 | 27 | 627 | 7 | 635 | 7 | 99 |
| ZR75 | 9 | 87 | 0.4 | 0.873 | 0.012 | 0.1023 | 0.0012 | 0.84 | 672 | 27 | 628 | 7 | 637 | 7 | 99 |
| ZR66 | 32 | 297 | 0.4 | 0.941 | 0.012 | 0.1024 | 0.0012 | 0.90 | 827 | 24 | 628 | 7 | 673 | 6 | 93 |
| ZR94 | 28 | 277 | 0.3 | 0.876 | 0.011 | 0.1026 | 0.0012 | 0.93 | 673 | 24 | 630 | 7 | 639 | 6 | 99 |
| ZR79 | 58 | 577 | 0.3 | 0.863 | 0.010 | 0.1027 | 0.0012 | 0.97 | 637 | 23 | 630 | 7 | 632 | 6 | 100 |
| ZR19 | 38 | 390 | 0.1 | 0.867 | 0.011 | 0.1035 | 0.0012 | 0.92 | 630 | 24 | 635 | 7 | 634 | 6 | 100 |
| ZR25 | 45 | 429 | 0.3 | 0.893 | 0.011 | 0.1035 | 0.0012 | 0.95 | 693 | 23 | 635 | 7 | 648 | 6 | 98 |
| ZR43 | 19 | 178 | 0.5 | 0.863 | 0.011 | 0.1035 | 0.0012 | 0.91 | 621 | 25 | 635 | 7 | 632 | 6 | 101 |
| ZR69 | 29 | 271 | 0.4 | 0.881 | 0.011 | 0.1037 | 0.0012 | 0.91 | 660 | 24 | 636 | 7 | 641 | 6 | 99 |
| ZR33 | 14 | 131 | 0.3 | 1.001 | 0.014 | 0.1041 | 0.0012 | 0.84 | 922 | 26 | 638 | 7 | 704 | 7 | 91 |
| ZR71 | 52 | 463 | 0.5 | 0.903 | 0.011 | 0.1047 | 0.0012 | 0.93 | 694 | 24 | 642 | 7 | 653 | 6 | 98 |
| ZR91 | 22 | 163 | 1.0 | 0.883 | 0.011 | 0.1048 | 0.0012 | 0.91 | 645 | 25 | 642 | 7 | 643 | 6 | 100 |
| ZR55 | 18 | 153 | 0.6 | 0.900 | 0.011 | 0.1052 | 0.0012 | 0.89 | 676 | 25 | 645 | 7 | 652 | 6 | 99 |
| ZR90 | 13 | 118 | 0.5 | 0.926 | 0.012 | 0.1060 | 0.0012 | 0.86 | 721 | 26 | 649 | 7 | 666 | 7 | 98 |
| ZR86 | 29 | 220 | 1.1 | 0.965 | 0.012 | 0.1067 | 0.0012 | 0.92 | 794 | 23 | 654 | 7 | 686 | 6 | 95 |
| ZR7 | 62 | 560 | 0.4 | 0.929 | 0.011 | 0.1069 | 0.0012 | 0.93 | 710 | 24 | 655 | 7 | 667 | 6 | 98 |
| ZR102 | 71 | 709 | 0.0 | 0.923 | 0.011 | 0.1071 | 0.0012 | 0.93 | 692 | 23 | 656 | 7 | 664 | 6 | 99 |
| ZR11 | 15 | 126 | 0.6 | 0.932 | 0.013 | 0.1078 | 0.0012 | 0.79 | 698 | 29 | 660 | 7 | 669 | 7 | 99 |
| ZR50 | 31 | 298 | 0.1 | 0.950 | 0.012 | 0.1093 | 0.0012 | 0.92 | 710 | 24 | 669 | 7 | 678 | 6 | 99 |
| ZR34 | 37 | 351 | 0.2 | 0.945 | 0.011 | 0.1095 | 0.0012 | 0.94 | 695 | 23 | 670 | 7 | 676 | 6 | 99 |
| ZR64 | 12 | 100 | 0.6 | 0.991 | 0.013 | 0.1102 | 0.0013 | 0.85 | 782 | 26 | 674 | 7 | 699 | 7 | 96 |
| ZR14 | 12 | 104 | 0.5 | 0.955 | 0.014 | 0.1108 | 0.0013 | 0.80 | 692 | 29 | 678 | 7 | 681 | 7 | 100 |
| ZR53 | 18 | 160 | 0.3 | 0.963 | 0.012 | 0.1130 | 0.0013 | 0.92 | 668 | 24 | 690 | 7 | 685 | 6 | 101 |
| ZR37 | 16 | 130 | 0.5 | 0.999 | 0.013 | 0.1136 | 0.0013 | 0.88 | 734 | 25 | 694 | 8 | 703 | 7 | 99 |
| ZR80 | 8 | 68 | 0.4 | 1.031 | 0.014 | 0.1150 | 0.0013 | 0.85 | 776 | 26 | 702 | 8 | 720 | 7 | 98 |
| ZR109 | 17 | 154 | 0.2 | 1.004 | 0.012 | 0.1163 | 0.0013 | 0.92 | 697 | 24 | 709 | 8 | 706 | 6 | 100 |
| ZR10 | 60 | 555 | 0.0 | 1.036 | 0.013 | 0.1165 | 0.0013 | 0.93 | 758 | 23 | 710 | 8 | 722 | 6 | 98 |
| ZR17 | 40 | 337 | 0.3 | 1.062 | 0.013 | 0.1172 | 0.0013 | 0.94 | 798 | 23 | 714 | 8 | 735 | 6 | 97 |
| ZR45 | 28 | 234 | 0.3 | 1.025 | 0.013 | 0.1183 | 0.0014 | 0.92 | 704 | 24 | 721 | 8 | 717 | 6 | 101 |
| ZR96 | 13 | 102 | 0.6 | 1.090 | 0.014 | 0.1190 | 0.0014 | 0.88 | 821 | 25 | 725 | 8 | 749 | 7 | 97 |
| ZR42 | 10 | 64 | 1.2 | 1.082 | 0.016 | 0.1208 | 0.0014 | 0.80 | 773 | 28 | 735 | 8 | 744 | 8 | 99 |
| ZR67 | 20 | 158 | 0.5 | 1.069 | 0.014 | 0.1210 | 0.0014 | 0.89 | 746 | 25 | 736 | 8 | 738 | 7 | 100 |
| ZR15 | 23 | 192 | 0.3 | 1.090 | 0.015 | 0.1223 | 0.0014 | 0.84 | 762 | 27 | 744 | 8 | 748 | 7 | 99 |
| ZR106 | 26 | 198 | 0.5 | 1.096 | 0.013 | 0.1232 | 0.0014 | 0.94 | 760 | 23 | 749 | 8 | 752 | 6 | 100 |
| ZR93 | 34 | 254 | 0.4 | 1.231 | 0.015 | 0.1247 | 0.0014 | 0.92 | 975 | 23 | 757 | 8 | 815 | 7 | 93 |
| ZR49 | 18 | 136 | 0.5 | 1.155 | 0.014 | 0.1251 | 0.0014 | 0.92 | 836 | 23 | 760 | 8 | 779 | 7 | 98 |
| ZR26 | 16 | 123 | 0.5 | 1.113 | 0.015 | 0.1255 | 0.0014 | 0.87 | 753 | 26 | 762 | 8 | 760 | 7 | 100 |

**TABLE III.** Continued

| | | | | Isotopic Ratios | | | | | Apparent Ages | | | | | | |
|---|---|---|---|---|---|---|---|---|---|---|---|---|---|---|---|
| PC7 | Pb (ppm) | U (ppm) | Th/U | 207Pb/235U | 1sigAbsErr | 206Pb/238U | 1sigAbsErr | rho | 207Pb/206Pb | 1sigAbsErr | 206Pb/238U | 1sigAbsErr | 207Pb/235U | 1sigAbsErr | Conc.(%) |
| ZR24 | 33 | 249 | 0.4 | 1.136 | 0.013 | 0.1268 | 0.0014 | 0.95 | 773 | 23 | 770 | 8 | 771 | 6 | 100 |
| ZR58 | 12 | 78 | 1.1 | 1.131 | 0.015 | 0.1269 | 0.0015 | 0.87 | 762 | 25 | 770 | 8 | 768 | 7 | 100 |
| ZR85 | 17 | 120 | 0.6 | 1.179 | 0.015 | 0.1298 | 0.0015 | 0.91 | 802 | 24 | 787 | 9 | 791 | 7 | 100 |
| ZR99 | 15 | 111 | 0.5 | 1.193 | 0.015 | 0.1305 | 0.0015 | 0.89 | 815 | 24 | 791 | 9 | 797 | 7 | 99 |
| ZR2 | 42 | 280 | 0.7 | 1.221 | 0.015 | 0.1326 | 0.0015 | 0.94 | 832 | 23 | 803 | 8 | 810 | 7 | 99 |
| ZR78 | 43 | 327 | 0.3 | 1.201 | 0.014 | 0.1329 | 0.0015 | 0.96 | 792 | 22 | 804 | 9 | 801 | 7 | 100 |
| ZR40 | 19 | 141 | 0.3 | 1.226 | 0.016 | 0.1331 | 0.0015 | 0.90 | 833 | 24 | 806 | 9 | 813 | 7 | 99 |
| ZR108 | 31 | 222 | 0.4 | 1.225 | 0.015 | 0.1341 | 0.0015 | 0.94 | 814 | 23 | 811 | 9 | 812 | 7 | 100 |
| ZR44 | 32 | 202 | 0.8 | 1.262 | 0.016 | 0.1349 | 0.0015 | 0.92 | 864 | 24 | 816 | 9 | 829 | 7 | 98 |
| ZR65 | 9 | 66 | 0.4 | 1.247 | 0.017 | 0.1350 | 0.0016 | 0.86 | 837 | 26 | 817 | 9 | 822 | 8 | 99 |
| ZR97 | 11 | 76 | 0.3 | 1.264 | 0.017 | 0.1370 | 0.0016 | 0.87 | 836 | 25 | 827 | 9 | 830 | 8 | 100 |
| ZR95 | 34 | 227 | 0.5 | 1.281 | 0.016 | 0.1384 | 0.0016 | 0.94 | 842 | 23 | 836 | 9 | 837 | 7 | 100 |
| ZR9 | 11 | 73 | 0.4 | 1.352 | 0.018 | 0.1411 | 0.0016 | 0.86 | 914 | 25 | 851 | 9 | 868 | 8 | 98 |
| ZR82 | 32 | 195 | 0.8 | 1.314 | 0.016 | 0.1418 | 0.0016 | 0.94 | 844 | 22 | 855 | 9 | 852 | 7 | 100 |
| ZR92 | 87 | 599 | 0.3 | 1.353 | 0.016 | 0.1421 | 0.0016 | 0.96 | 901 | 22 | 857 | 9 | 869 | 7 | 99 |
| ZR83 | 94 | 627 | 0.4 | 1.412 | 0.017 | 0.1447 | 0.0017 | 0.97 | 951 | 21 | 871 | 9 | 894 | 7 | 97 |
| ZR62 | 31 | 219 | 0.2 | 1.376 | 0.017 | 0.1451 | 0.0017 | 0.92 | 893 | 23 | 874 | 9 | 879 | 7 | 99 |
| ZR4 | 26 | 178 | 0.2 | 1.401 | 0.017 | 0.1470 | 0.0016 | 0.92 | 902 | 23 | 884 | 9 | 889 | 7 | 99 |
| ZR31 | 50 | 304 | 0.7 | 1.429 | 0.017 | 0.1472 | 0.0017 | 0.96 | 940 | 22 | 885 | 9 | 901 | 7 | 98 |
| ZR39 | 31 | 197 | 0.3 | 1.512 | 0.019 | 0.1567 | 0.0018 | 0.93 | 927 | 23 | 939 | 10 | 935 | 8 | 100 |
| ZR28 | 64 | 346 | 0.9 | 1.532 | 0.018 | 0.1572 | 0.0018 | 0.97 | 949 | 22 | 941 | 10 | 943 | 7 | 100 |
| ZR105 | 89 | 395 | 1.8 | 1.580 | 0.019 | 0.1586 | 0.0018 | 0.93 | 993 | 22 | 949 | 10 | 962 | 8 | 99 |
| ZR104 | 46 | 261 | 0.6 | 1.557 | 0.019 | 0.1594 | 0.0018 | 0.93 | 954 | 23 | 953 | 10 | 953 | 8 | 100 |
| ZR70 | 44 | 219 | 1.2 | 1.582 | 0.019 | 0.1595 | 0.0018 | 0.93 | 985 | 23 | 954 | 10 | 963 | 8 | 99 |
| ZR76 | 62 | 363 | 0.5 | 1.578 | 0.019 | 0.1597 | 0.0018 | 0.97 | 977 | 21 | 955 | 10 | 962 | 7 | 99 |
| ZR6 | 59 | 348 | 0.4 | 1.599 | 0.019 | 0.1608 | 0.0018 | 0.93 | 989 | 22 | 961 | 10 | 970 | 8 | 99 |
| ZR47 | 46 | 247 | 0.7 | 1.612 | 0.019 | 0.1633 | 0.0018 | 0.94 | 975 | 22 | 975 | 10 | 975 | 8 | 100 |
| ZR111 | 29 | 169 | 0.4 | 1.615 | 0.019 | 0.1633 | 0.0019 | 0.94 | 978 | 22 | 975 | 10 | 976 | 8 | 100 |
| ZR89 | 28 | 153 | 0.6 | 1.676 | 0.021 | 0.1681 | 0.0019 | 0.92 | 995 | 23 | 1002 | 11 | 999 | 8 | 100 |
| ZR115 | 27 | 134 | 1.0 | 1.682 | 0.021 | 0.1674 | 0.0019 | 0.90 | 1010 | 24 | 998 | 11 | 1002 | 8 | 99 |
| ZR114 | 44 | 247 | 0.4 | 1.739 | 0.021 | 0.1723 | 0.0020 | 0.95 | 1019 | 22 | 1025 | 11 | 1023 | 8 | 100 |
| ZR112 | 16 | 96 | 0.6 | 1.557 | 0.024 | 0.1538 | 0.0018 | 0.76 | 1026 | 29 | 922 | 10 | 953 | 10 | 93 |
| ZR29 | 28 | 162 | 0.7 | 1.590 | 0.020 | 0.1565 | 0.0018 | 0.92 | 1033 | 23 | 937 | 10 | 966 | 8 | 94 |
| ZR81 | 12 | 94 | 0.9 | 1.062 | 0.015 | 0.1014 | 0.0012 | 0.81 | 1095 | 27 | 622 | 7 | 735 | 8 | 67 |
| ZR59 | 41 | 190 | 1.3 | 1.952 | 0.023 | 0.1661 | 0.0019 | 0.94 | 1321 | 21 | 990 | 10 | 1099 | 8 | 83 |
| ZR88 | 17 | 108 | 0.2 | 2.063 | 0.025 | 0.1416 | 0.0016 | 0.93 | 1726 | 20 | 854 | 9 | 1137 | 8 | 66 |
| ZR22 | 84 | 319 | 0.4 | 3.649 | 0.042 | 0.2448 | 0.0028 | 0.98 | 1769 | 19 | 1411 | 14 | 1560 | 9 | 88 |
| ZR73 | 40 | 284 | 0.5 | 1.861 | 0.024 | 0.1187 | 0.0014 | 0.90 | 1860 | 21 | 723 | 8 | 1067 | 9 | 57 |
| ZR46 | 53 | 142 | 0.7 | 5.056 | 0.059 | 0.3222 | 0.0036 | 0.97 | 1862 | 19 | 1800 | 18 | 1829 | 10 | 98 |
| ZR21 | 163 | 563 | 0.3 | 4.570 | 0.052 | 0.2753 | 0.0031 | 0.99 | 1962 | 18 | 1568 | 16 | 1744 | 10 | 89 |
| ZR57 | 74 | 202 | 0.5 | 5.514 | 0.066 | 0.3311 | 0.0038 | 0.95 | 1968 | 19 | 1844 | 18 | 1903 | 10 | 97 |
| ZR87 | 605 | 2850 | 0.2 | 3.531 | 0.041 | 0.2012 | 0.0023 | 0.98 | 2061 | 18 | 1182 | 12 | 1534 | 9 | 74 |
| ZR60 | 230 | 697 | 0.1 | 5.744 | 0.067 | 0.3258 | 0.0037 | 0.97 | 2069 | 18 | 1818 | 18 | 1938 | 10 | 94 |
| ZR30 | 337 | 911 | 0.2 | 6.889 | 0.080 | 0.3599 | 0.0041 | 0.98 | 2213 | 18 | 1982 | 19 | 2097 | 10 | 95 |
| ZR103 | 314 | 1278 | 1.2 | 3.707 | 0.045 | 0.1850 | 0.0021 | 0.94 | 2292 | 19 | 1094 | 11 | 1573 | 10 | 69 |
| ZR36 | 178 | 407 | 0.1 | 9.683 | 0.113 | 0.4223 | 0.0048 | 0.97 | 2521 | 18 | 2271 | 22 | 2405 | 11 | 95 |
| ZR84 | 120 | 255 | 0.6 | 9.293 | 0.108 | 0.4042 | 0.0046 | 0.98 | 2525 | 17 | 2189 | 21 | 2367 | 11 | 94 |
| ZR48 | 177 | 389 | 0.2 | 10.240 | 0.117 | 0.4278 | 0.0048 | 0.98 | 2593 | 17 | 2296 | 22 | 2457 | 11 | 95 |
| ZR98 | 174 | 272 | 1.4 | 11.629 | 0.138 | 0.4743 | 0.0054 | 0.96 | 2633 | 18 | 2502 | 24 | 2575 | 11 | 98 |
| ZR100 | 98 | 121 | 2.3 | 12.429 | 0.148 | 0.5047 | 0.0057 | 0.95 | 2640 | 18 | 2634 | 25 | 2637 | 11 | 100 |
| ZR63 | 77 | 139 | 0.5 | 12.283 | 0.145 | 0.4859 | 0.0055 | 0.96 | 2684 | 18 | 2553 | 24 | 2626 | 11 | 98 |

**TABLE IV.** Operating conditions for the LA-ICP-MS equipment

| | |
|---|---|
| **Laboratory & Sample Preparation** | |
| Laboratory name | GeOHeLiS Analytical Platform, Géosciences Rennes/OSUR, Univ. Rennes |
| Sample type/mineral | zircon |
| Sample preparation | Conventional mineral separation, 1 inch resin mount, 1µm polish to finish |
| Imaging | (CL) imaging using a Quanta 200 SEM with centaurus detector at the Laboratoire Magmas d'océanologie et de geosciences, Université de Lille 1 (Lille, France). |
| **Laser ablation system** | |
| Make, Model & type | ESI NWR193UC, Excimer |
| Ablation cell | ESI NWR TwoVol2 |
| Laser wavelength | 193 nm |
| Pulse width | < 5 ns |
| Fluence | 7 J/cm-2 |
| Repetition rate | 5 Hz |
| Spot size | 25 µm |
| Sampling mode / pattern | Single spot |
| Carrier gas | 100% He, Ar make-up gas and N2 (3 ml/mn) combined using in-house smoothing device |
| Background collection | 20 seconds |
| Ablation duration | 60 seconds |
| Wash-out delay | 15 seconds |
| Cell carrier gas flow (He) | 0.75 l/min |
| **ICP-MS Instrument** | |
| Make, Model & type | Agilent 7700x, Q-ICP-MS |
| Sample introduction | Via conventional tubing |
| RF power | 1350W |
| Sampler, skimmer cones | Ni |
| Extraction lenses | X type |
| Make-up gas flow (Ar) | 0.85 l/min |
| Detection system | Single collector secondary electron multiplier |
| Data acquisition protocol | Time-resolved analysis |
| Scanning mode | Peak hopping, one point per peak |
| Detector mode | Pulse counting, dead time correction applied, and analog mode when signal intensity > ~ $10^6$ cps |
| Masses measured | $^{204}$(Hg + Pb), $^{206}$Pb, $^{207}$Pb, $^{208}$Pb, $^{232}$Th, $^{238}$U |
| Integration time per peak | 10-30 ms |
| Sensitivity / Efficiency | 20000 cps/ppm Pb (50µm, 10Hz) |
| **Data Processing** | |
| Gas blank | 20 seconds on-peak |
| Calibration strategy | GJ1 zircon standard used as primary reference material, Plešovice used as secondary reference material (quality control) |
| Reference Material info | GJ1 (Jackson et al., 2004)<br>Plešovice (Slama et al., 2008) |
| Data processing package used | GLITTER ® (van Achterbergh et al., 2001) |
| Quality control / Validation | Plešovice: concordia age = 336.7 ± 0.8 Ma (N=36; MSWD=0.33) |

**FIGURE I.**

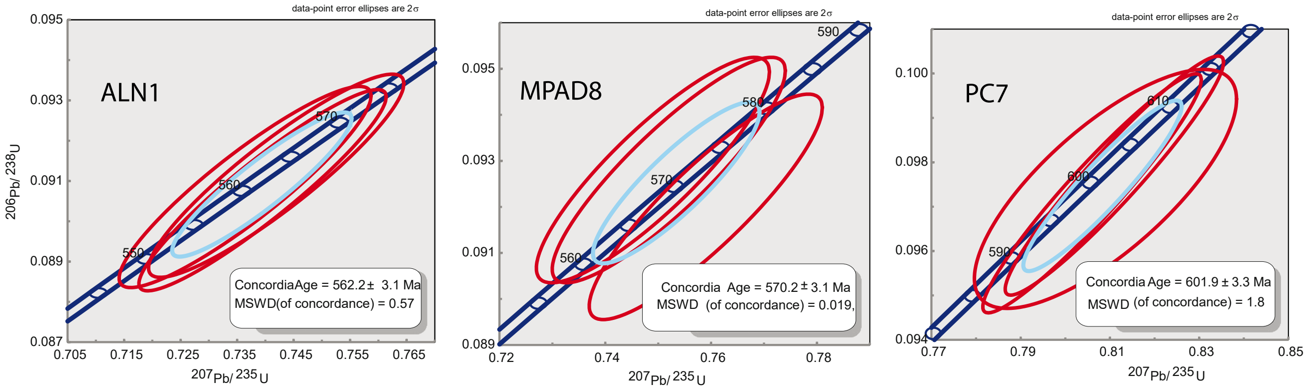
data-point error ellipses are 2σ
ALN1
ConcordiaAge = 562.2 ± 3.1 Ma
MSWD(of concordance) = 0.57
MPAD8
Concordia Age = 570.2 ± 3.1 Ma
MSWD (of concordance) = 0.019,
PC7
Concordia Age = 601.9 ± 3.3 Ma
MSWD (of concordance) = 1.8
206Pb/238U
207Pb/235U